Limnol. Oceanogr., 59(5), 2014, 1529–1554

doi:10.4319/lo.2014.59.5.1529

Effect of submarine groundwater discharge on the coastal ocean inorganic carbon cycle

Qian Liu,[1,2] Matthew A. Charette,[2,*] Paul B. Henderson,[2] Daniel C. McCorkle,[3] William Martin,[2] and Minhan Dai[1]

[1] State Key Lab of Marine Environmental Science, Xiamen University, Xiamen, Fujian, China
[2] Department of Marine Chemistry and Geochemistry, Woods Hole Oceanographic Institution, Woods Hole, Massachusetts
[3] Department of Geology and Geophysics, Woods Hole Oceanographic Institution, Woods Hole, Massachusetts

Abstract

Using radium (Ra) isotopes, we estimate that the average submarine groundwater discharge (SGD) flux (marine plus terrestrial groundwater) into the southwest Florida Shelf (SWFS) was $20 \pm 10 \times 10^7$ and $18 \pm 8 \times 10^7$ m^3 d^{-1} in July and October 2009, respectively. The terrestrial groundwater flux was the same order of magnitude as the local river discharge in July 2009. Shelf-water total alkalinity (TAlk) and dissolved inorganic carbon (DIC) concentrations could not be explained by river inputs alone, suggesting a groundwater source. We estimated SGD fluxes of TAlk and DIC using the SGD flux derived from a shelf-water ^{226}Ra budget and TAlk and DIC concentration differences between the groundwater and seawater. These fluxes were also determined by the observed TAlk : ^{226}Ra and DIC : ^{226}Ra relationships in the shelf water, and the ^{226}Ra flux sustained by SGD. These TAlk and DIC fluxes were 11–71 times more than the combined input of local rivers, suggesting that SGD was the dominant source of TAlk and DIC to the SWFS during 2009. SGD is an important component of the inorganic carbon budget for the coastal ocean.

Submarine groundwater discharge (SGD), defined as the flow of water from the seabed to the ocean along continental margins, includes both terrestrial and marine groundwater from seawater exchange through the coastal aquifer (Burnett et al. 2003). This process is thought to occur in all permeable coastal aquifers, both unconfined and confined (Johannes 1980); there is growing recognition that SGD is an important component of land–ocean interactions. Although the flux of SGD at global scales remains difficult to precisely constrain, recent studies have suggested that the total volume flux of terrestrial SGD is ~ 5–10% of the amount of water supplied to the ocean by rivers (Burnett et al. 2003).

It has been well documented that SGD affects the biogeochemical cycling of nutrients and trace metals in the coastal ocean. For example, SGD has been shown to be the major nutrient source for triggering harmful algal blooms in the southern sea of Korea (Lee et al. 2010), and iron fluxes from SGD along the southeast coastline of Brazil were 10% of the atmospheric flux to the entire South Atlantic Ocean (Windom et al. 2006).

Groundwater is often enriched in carbon dioxide (CO_2) due to organic carbon degradation within coastal aquifers (Gagan et al. 2002). Studies have shown that the partial pressure of CO_2 (P_{CO_2}) in groundwater can be as high as ~ 12,000 Pa, or three orders of magnitude higher than atmospheric CO_2 (Gagan et al. 2002; Cai et al. 2003). When discharged, these CO_2-enriched groundwaters shall certainly influence the carbon dynamics and budget for the coastal ocean. A strong link between SGD and P_{CO_2} in coastal waters has indeed been previously observed (e.g., Australia; Santos et al. 2012). In the South Atlantic Bight, Cai et al. (2003) found that the flux of dissolved inorganic carbon (DIC) from groundwater was comparable with the riverine flux. In the Okatee estuary, SGD-derived DIC fluxes exceeded river DIC inputs to the estuary (Moore et al. 2006). Even in a river-dominated shelf system in the northern South China Sea, the SGD-delivered DIC flux was ~ 30% of the DIC load carried by the Pearl River (Liu et al. 2012). Nevertheless, there have been a limited number of quantitative, process-oriented studies on the DIC flux through SGD.

The southwest Florida Shelf (SWFS) is a subtropical carbonate platform often overlying karstic limestone comprised of abundant fossil mollusk and calcareous and coralline algae (Brooks et al. 2003). Karst aquifers often have higher than average porosity due to calcium carbonate dissolution, which facilitates SGD transport to the coastal ocean through conduit flow (Fleury et al. 2007). Therefore, SGD is generally important in karst regions (Fleury et al. 2007), and in addition, the SWFS is characterized by very limited river discharge. Here, we use radium (Ra) isotopes to demonstrate that the SWFS is a groundwater-dominated shelf, and that the SGD-associated total alkalinity (TAlk) and DIC fluxes exceed carbon sources from rivers and sediment diffusion.

Methods

Study site—The SWFS is one of the broadest continental shelves in the North America, with a low shelf gradient of 0.2–4 m km^{-1} (Hine et al. 2008). Our study region includes the southern portion of the SWFS, extending from the Florida Keys in the south to Tampa Bay in the north (Fig. 1). The isobaths generally run parallel to the coastline (Yang et al. 1999), with the northern shelf being narrower than the southern portion (Fig. 1). A noteworthy feature of the SWFS geology is the presence of phosphate deposits (Burnett 1998), which contain high amounts of uranium (U) and U-decay series daughters (Burnett 1998), e.g., ^{238}U,

* Corresponding author: mcharette@whoi.edu

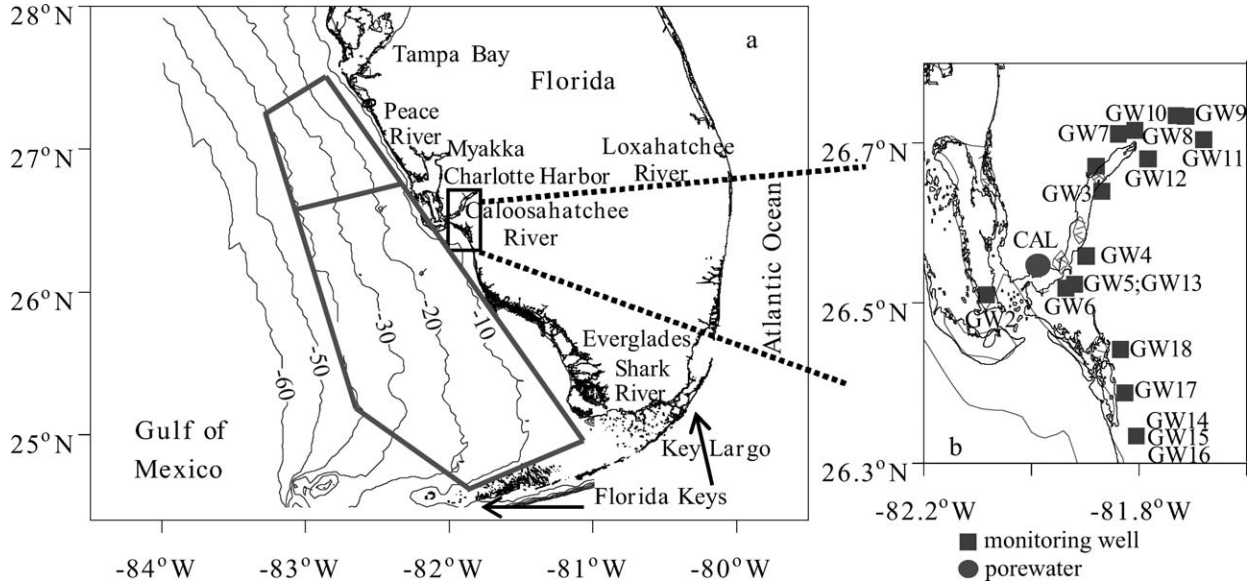

Fig. 1. (a) Bathymetric map (depth in m) of the southwest Florida Shelf, and (b) groundwater sampling carried out from 17 to 27 July and 05 to 14 October 2009. The gray domain represents the region of our box model; surface-water station locations over the shelf are shown in Fig. 2. Groundwater sampling sites were collected near the Caloosahatchee River estuary in April and October in 2009 and 2010. Square symbols represent monitoring wells, and the filled circle denotes the location of a series of shallow groundwater samples collected via piezometers.

^{226}Ra. Several small rivers drain into the SWFS: the Shark River and Caloosahatchee River directly discharge into the SWFS, while the Peace and Myakka Rivers converge at Charlotte Harbor, and the Hillsborough, Alafia, and Little Manatee flow into Tampa Bay.

The limestone foundation of the SWFS facilitates the formation of fresh and saline springs. However, regional-scale estimates of SGD for the SWFS are scarce. Smith and Swarzenski (2012) derived a groundwater nitrogen flux to the inner shelf (10 m isobath) that was 7–150 times greater than the estuarine flux from Tampa Bay. More common are SGD studies that focused on local estuaries along this shelf (Swarzenski et al. 2007). While these studies demonstrated the significance of SGD to the estuarine and shelf ecosystem, the SWFS remains an unexplored territory with respect to SGD's role in the inorganic carbon cycle.

Sampling and analysis—Two surveys of the SWFS were conducted aboard the R/V *F. G. Walton Smith* from 17 to 27 July and 05 to 14 October 2009. Seven shore-perpendicular transects (CH1, CR1, CR1a, CR1b, CR1c, EG1, and EG2 in Fig. 2a), off Charlotte Harbor in the north and the Everglades to the south, were completed in July. One additional transect off Tampa Bay was carried out in October, for a total eight transects (TB, CH2, CH3, CR2, CR3, CR3a, EG3, and EG4 in Fig. 2b). Our study was focused on the shelf extending out to the 70 m isobath, which ranged from 95–180 km offshore. In addition to shelf water, we collected samples in the local estuaries during the two cruises. The Shark River estuary (SRE) was sampled in July, and Tampa Bay, Charlotte Harbor, and the Caloosahatchee River estuary (CRE) were sampled in October. Based on the monthly rainfall and river discharge rate in 2009 (Fig. 3), May marked the start of the wet season and October was the beginning of dry season; thus, our sampling program was entirely within the wet season. The groundwater table and hydraulic gradient between groundwater level and seawater were higher in the wet season compared with dry season (Fig. 3).

Large-volume (80–210 liters) filtered (1 μm) seawater ($\sim$ 2 m below the surface) samples were pumped into plastic drums to measure Ra (^{223}Ra, ex ^{224}Ra, ^{228}Ra, ^{226}Ra). Deeper samples for Ra, TAlk, and DIC were collected by multiple 30 liter Niskin bottles mounted on a rosette equipped with a calibrated Sea-Bird Electronics (SBE)-19-plus conductivity–temperature–depth recorder. Separate salinity samples were stored in glass bottles and were analyzed by a Guideline salinometer. Samples for TAlk and DIC were stored in 150 mL borosilicate glass vials and poisoned upon collection with 50 μL of a saturated $HgCl_2$ solution.

We collected groundwater samples (Fig. 1b) from monitoring wells along the CRE and piezometers (MHE Products Push Point sampler) in the beach during April and October in 2009 and 2010. A peristaltic pump was connected to a flow-through cell containing a YSI (Yellow Springs Instrument Company) 600XLM sonde. When salinity, temperature, and dissolved oxygen readings became constant, we collected samples for Ra (10–25 liters), TAlk, and DIC. As a check on the YSI calibration, separate water samples were collected for salinity and analyzed by a Guideline salinometer. Suspended particles in the freshwater (salinity < 0.3) reaches of the CRE were collected on a 1 μm Hytrex polypropylene cartridge for measurement of ^{226}Ra. The filter was dried, ashed, and analyzed via gamma spectrometry.

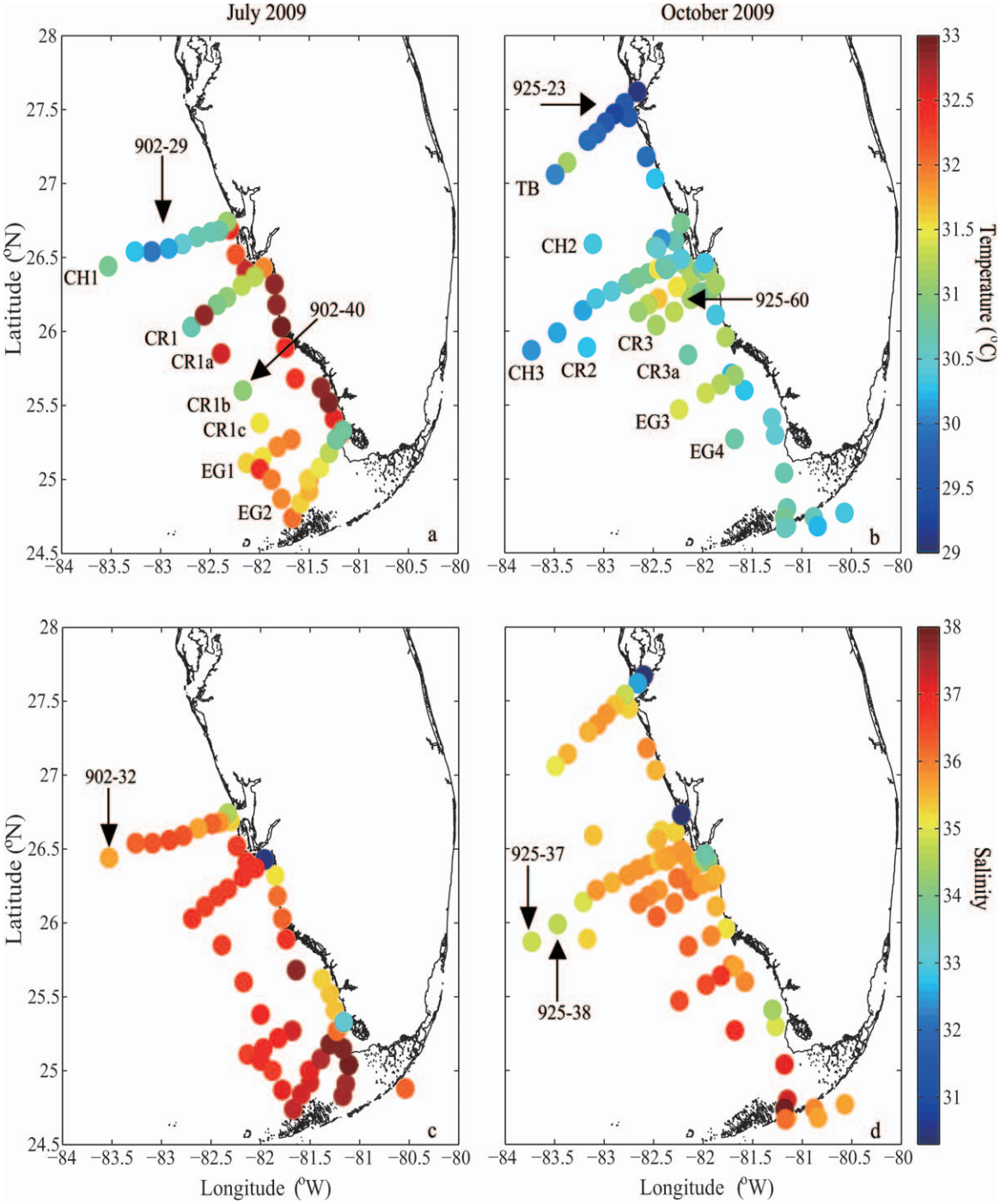

Fig. 2. Temperature (°C) and salinity distributions in the surface water of southwest Florida Shelf sampled in (a, c) July and (b, d) October 2009. Also shown are the shore-perpendicular transect identification numbers for July and October.

We passed the Ra samples through MnO_2-impregnated acrylic fibers at flow rate < 1 L min^{-1} to quantitatively adsorb Ra onto MnO_2 (Charette et al. 2001). We then rinsed the fibers with deionized water to remove salts, adjusted the fiber moisture content with compressed air, and placed the fibers in a Radium Delayed Coincidence Counter system to determine the short-lived radium isotopes, ^{223}Ra ($T_{1/2}$ = 11.4 d) and ^{224}Ra ($T_{1/2}$ = 3.7 d; Moore and Arnold 1996). The detailed measurement procedures are presented in Liu et al. (2012). After determining short-lived Ra isotope activities, the Mn fibers were ashed at 820°C for 22 h, homogenized, and placed in counting vials sealed with epoxy for ^{222}Rn ingrowth at least 3 weeks prior to counting (Charette et al. 2001). The ash was placed in a well-type gamma spectrometer (model GCW4023, Canberra) to measure long-lived Ra, ^{226}Ra ($T_{1/2}$ = 1600 yr), and ^{228}Ra ($T_{1/2}$ = 5.75 yr). Each detector was standardized by use of National Institute of Standards

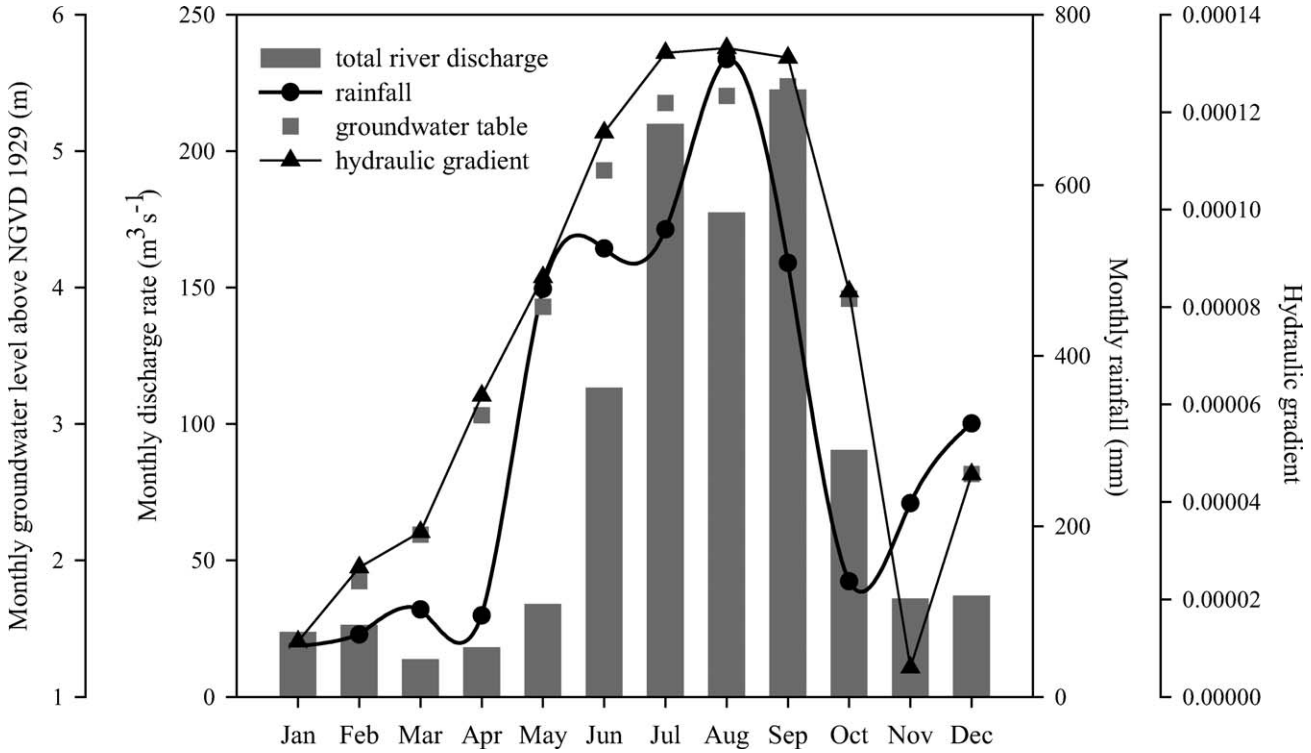

Fig. 3. Monthly groundwater table above National Geodetic Vertical Datum of 1929 (NGVD 29) from Naples, Florida (United States Geological Survey [USGS] well No. 262248081314101-C-1244; latitude 26°22′48″, longitude −81°31′41″), hydraulic gradient between groundwater level and sea level at Naples (horizontal distance from the monitoring well to the tidal bench mark is 21 km; sea level data were downloaded from http://tidesandcurrents.noaa.gov/data_menu.shtml?extremetype=monthly&bdate=20090101&edate=20091231&unit=0&format=Apply+Change&stn=8725110+Naples%2C+FL&type=Extremes), total monthly rainfall in the main watershed of the southwest Florida Shelf including the Peace River basin, Myakka River basin, Caloosahatchee River basin, and Everglades watershed in 2009. All of the river flow rates were downloaded from the USGS Web site "USGS Surface-Water Data for the Nation" (http://waterdata.usgs.gov/nwis/sw) and the respective gauge stations are listed in Table 5.

and Technology–certified reference materials prepared in the same geometry as the samples (Charette et al. 2001).

DIC was determined by acidification of 0.5 mL of a water sample with phosphoric acid to drive off CO_2, which was quantified with a nondispersive infrared detector (Li-Cor 6252). TAlk was determined by the Gran titration method using a Metrohm 808 Titrando with 1 mL burette. Both DIC and TAlk were calibrated against certified reference materials from A. Dickson of the Scripps Institution of Oceanography. The analytical precision was 3 μmol kg^{-1} for DIC and 4 μmol kg^{-1} for TAlk.

Results

Basic hydrological characteristics—The salinity of surface water in our study domain ranged from 30.49 to 37.93 (mean 36.26) in July (Fig. 2c; Table 1) and 30.40 to 37.18 (mean 35.47) in October (Fig. 2d; Table 1). Low salinities observed in the nearshore region were influenced by river discharge in these two months. The peak in total major river discharge along the SWFS in 2009 was from June to October (Fig. 3). However, we also observed several relatively low salinity sites located in the offshore region (e.g., Fig. 2c,d, sites 902-32, 925-37, 925-38), which may be due to the southward advection of river plume discharge from the northern of Gulf of Mexico (Morey et al. 2003). Stratification was similar for July and October for most of the stations. The water column was well mixed shoreward of the 10 m isobath, while the mixed-layer thickness generally increased with distance offshore ranging from 12 to 40 m. During these two cruises, we found several instances of an abnormal vertical salinity distribution at inner and middle shelf stations. At sites 902-29, 902-40, and 925-23, salinity minima were found near the bottom of the water column (dashed line in Fig. 4). Although only a few hundredths of salinity unit different from surface water, these anomalies suggest a possible local influence of springs or diffusive groundwater input. The temperature of surface water ranged from 29.98°C to 33.08°C (mean 31.69°C) in July (Fig. 2a) and from 29.08°C to 31.65°C (mean 30.72°C) in October (Fig. 2b). The average temperature in July was 0.96°C higher than in October. Slightly higher temperatures were observed in the bottom water of inner shelf site 925-60 (Fig. 4), close to the location of the geothermal spring seepage zone (Fanning et al. 1981).

Ra isotopes in the groundwater, estuaries, and shelf water—Ra activity in the groundwater: Groundwater salinity along the CRE ranged from 0.2 to 40.2 (Table 2), with most of the monitoring wells having lower salinity (ranging 0.2–5.4) with the exception of a hypersaline well (GW2) with salinity of 32–40. The salinity of the beach

Table 1. Radium activities, total alkalinity (TAlk), dissolved inorganic carbon (DIC), and water age at sampling sites for the southwest Florida Shelf, Shark River estuary, Tampa Bay, Charlotte Harbor, and Caloosahatchee River estuary in July and October 2009*. Dashes indicate no data.

Station	Salinity	^{223}Ra (Bq m^{-3})	ex ^{224}Ra (Bq m^{-3})	^{228}Ra (Bq m^{-3})	± (Bq m^{-3})	^{226}Ra (Bq m^{-3})	± (Bq m^{-3})	TAlk (μmol L^{-1})	DIC (μmol L^{-1})	Water age (d)
Southwest Florida Shelf, July 2009										
902-2	37.6	0.3	1.6	1.9	0.2	6.0	0.1	2375	1945	11
902-3	37.6	0.3	1.3	2.6	0.2	7.6	0.1	2411	2055	18
902-4	37.9	0.3	0.8	1.6	0.1	4.0	0.1	2502	2162	9
902-5	37.8	0.4	1.4	2.3	0.2	5.4	0.1	2459	2134	11
902-6	35.0	2.8	5.1	12.0	0.2	22.5	0.1	2741	2473	13
902-7	35.4	1.7	3.1	11.3	0.2	20.3	0.1	2713	2352	20
902-8	35.4	1.5	2.0	10.5	0.4	19.3	0.2	2737	2340	21
902-9	35.2	1.8	2.8	9.9	0.1	16.6	0.1	2787	2332	17
902-10	37.6	1.4	1.8	5.5	0.2	10.3	0.1	2568	2167	11
902-12	36.8	1.3	2.1	6.4	0.1	13.6	0.1	2504	2136	14
902-13	36.3	1.3	1.7	5.1	0.2	11.3	0.1	2511	2131	9
902-14	36.2	0.7	1.1	3.4	0.2	7.2	0.1	2526	2145	11
902-15	35.1	1.0	1.6	2.9	0.3	6.9	0.2	2558	2182	3
902-16	35.0	2.1	3.1	5.3	0.3	11.8	0.2	2509	2160	3
902-17	36.7	2.7	3.0	8.2	0.3	16.1	0.2	2527	2184	7
902-18	36.6	2.6	3.2	6.2	0.2	12.1	0.1	2483	2120	2
902-19	35.3	4.4	5.1	13.8	0.7	25.1	0.4	2451	2122	7
902-24	34.6	1.7	2.4	6.0	0.1	10.5	0.2	2484	2129	8
902-25	35.8	0.6	0.9	3.0	0.3	5.7	0.2	2478	2115	12
902-26	36.2	0.3	0.4	2.4	0.1	4.9	0.1	2474	2122	19
902-27	35.7	0.2	0.2	2.0	0.1	3.8	0.0	2479	2116	21
902-28	36.4	0.1	0.2	2.0	0.1	3.9	0.1	2474	2118	40
902-28-23m	36.4	0.1	0.4	1.5	0.2	3.4	0.1	2463	2186	—
902-28-15m	36.3	0.1	0.1	1.7	0.1	3.2	0.1	2491	2211	—
902-29	36.4	0.1	0.2	1.3	0.2	2.5	0.1	2458	2099	25
902-30	36.4	0.0	0.2	0.7	0.1	1.3	0.0	2443	2086	—
902-31	36.2	0.0	0.1	0.8	0.1	1.1	0.1	2436	2078	—
902-32	35.7	0.0	0.2	1.1	0.1	1.3	0.1	2427	2071	58
902-32-55m	36.5	0.0	0.5	1.2	0.2	2.2	0.1	2469	2145	—
902-33	36.8	0.0	0.2	1.3	0.1	2.7	0.0	2463	2102	38
902-33-30m	36.5	0.2	0.6	1.1	0.2	3.1	0.1	2521	2171	—
902-33.5	30.5	2.5	4.5	5.7	0.2	13.9	1.0	2561	2247	0
902-34	36.7	1.1	1.2	4.6	0.3	8.7	0.2	2514	2136	10
902-35	36.7	0.8	1.0	5.2	0.1	10.3	0.1	2496	2128	19
902-36	36.6	0.4	0.7	2.2	0.2	5.2	0.1	2466	2099	10
902-37	36.6	0.2	0.6	2.0	0.1	5.0	0.1	2461	2089	18
902-38	36.6	0.1	0.2	1.9	0.1	4.1	0.1	2472	2108	34
902-39	36.6	0.1	0.1	1.5	0.1	3.5	0.1	2456	2087	33
902-39-24m	36.5	0.2	0.4	1.4	0.1	3.5	0.1	2444	2112	—
902-40	36.7	0.1	0.4	0.8	0.1	3.1	0.1	2459	2113	—
902-41	37.2	0.3	0.5	2.9	0.1	8.5	0.1	2519	2149	23
902-42	37.0	0.3	0.7	3.6	0.1	11.3	0.1	2451	2083	27
902-42-15m	37.0	0.2	0.6	2.8	0.2	8.2	0.1	2477	2107	—
902-43	37.3	0.2	0.5	3.0	0.1	8.8	0.1	2474	1966	34
902-44	37.2	0.3	0.6	2.9	0.2	8.3	0.1	2491	2113	25
902-44-11m	37.1	0.3	0.7	3.2	0.3	8.2	0.2	2496	2107	—
902-45	37.0	0.2	0.4	2.8	0.2	7.9	0.1	2485	2134	25
902-46	36.9	0.1	0.4	2.1	0.1	6.4	0.1	2419	2183	34
902-47	36.6	0.2	0.5	2.4	0.1	7.2	0.1	2404	2159	23
902-48	36.8	0.1	0.3	1.9	0.2	6.4	0.1	2398	2172	27
902-49	36.7	0.2	0.4	1.6	0.1	4.9	0.1	2358	2137	19
902-49-19m	36.7	0.2	0.4	1.7	0.1	5.5	0.1	2477	2136	—
902-50	37.0	0.1	0.4	1.8	0.1	4.9	0.1	2474	2130	23
902-51	37.4	0.2	0.7	1.9	0.1	6.9	0.1	2376	1983	17
902-52	37.2	0.1	0.4	0.8	0.1	2.6	0.0	2490	2141	—
902-53	37.2	0.1	0.5	1.5	0.1	4.5	0.1	2451	2102	18
902-54	37.1	0.3	0.6	3.1	0.2	8.5	0.1	2479	2007	27
902-55	37.4	0.3	0.9	2.5	0.2	6.9	0.1	2449	2089	21

Table 1. Continued.

Station	Salinity	^{223}Ra (Bq m^{-3})	ex ^{224}Ra (Bq m^{-3})	^{228}Ra (Bq m^{-3})	± (Bq m^{-3})	^{226}Ra (Bq m^{-3})	± (Bq m^{-3})	TAlk (μmol L^{-1})	DIC (μmol L^{-1})	Water age (d)
902-56	37.8	0.4	1.3	3.8	0.4	9.3	0.2	2497	2117	22
902-57	36.1	0.8	2.0	5.8	0.2	11.1	0.1	2602	2306	20
Shark River estuary										
902-58	33.2	4.1	7.8	14.3	0.3	26.0	0.1	2892	3215	—
902-59	30.1	7.3	11.8	15.6	1.6	32.5	0.9	3058	3498	—
902-61	11.1	3.6	7.8	9.6	0.8	22.6	0.4	3418	4016	—
902-63	0.4	0.4	0.7	1.7	0.5	7.6	0.2	2780	3251	—
902-65	0.2	0.1	0.4	1.8	0.8	6.3	0.4	2535	—	—
902-67	0.2	0.0	0.5	—	—	5.4	0.4	2646	3269	—
902-79	—	5.7	9.6	16.7	1.5	33.4	0.8	—	—	—
Southwest Florida Shelf, October 2009										
925-2	35.6	0.1	0.2	0.9	0.2	2.4	0.1	2391	2040	—
925-3	37.2	0.3	0.2	2.1	0.3	6.9	0.2	2234	1908	6
925-4	37.1	0.4	0.1	2.1	0.3	7.3	0.2	2369	2033	5
925-5	34.9	0.8	0.1	6.6	0.6	14.2	0.4	2513	2205	20
925-6	34.5	1.1	0.1	4.6	0.5	9.8	0.3	2543	2225	6
925-7	35.9	0.5	0.1	5.7	0.5	11.5	0.3	2449	2089	27
925-8	35.9	0.8	0.1	5.4	0.7	11.1	0.4	2538	2165	17
925-9	35.5	1.0	0.1	5.2	0.7	14.5	0.5	2577	2178	11
925-10	35.7	0.6	0.0	5.6	0.5	16.7	0.3	2530	2157	21
925-11	34.6	1.1	0.1	6.0	0.4	17.2	0.3	2564	2224	13
925-12	35.6	1.6	0.3	6.0	0.4	15.6	0.3	2481	2138	7
925-13	35.3	1.6	0.2	5.7	0.4	11.3	0.2	2448	2120	6
925-14	35.6	0.5	0.1	3.5	0.3	7.1	0.2	2457	2083	14
925-15	35.9	0.9	0.1	4.1	0.3	8.4	0.2	2477	2107	8
925-16	35.2	0.8	0.1	4.9	0.6	9.3	0.3	2453	2090	15
925-23	35.8	0.3	0.0	3.2	0.4	6.1	0.2	2433	2071	19
925-24	35.8	0.1	0.0	2.1	0.3	3.5	0.2	2424	2075	21
925-25	35.5	0.1	0.0	1.4	0.2	2.3	0.1	2424	2075	7
925-26	35.5	0.0	0.0	0.9	0.1	1.9	0.1	2422	2065	—
925-27	35.1	0.0	0.0	1.2	0.2	1.7	0.1	2474	2076	38
925-28	34.7	0.0	0.0	1.1	0.1	1.1	0.0	2436	2066	—
925-29	35.3	0.2	0.1	2.6	0.4	5.2	0.2	2429	—	20
925-30	36.1	0.2	0.0	1.6	0.4	6.4	0.2	2443	—	0
925-31	35.8	0.5	0.0	4.9	0.5	14.3	0.3	2526	—	13
925-32	36.1	0.4	0.1	2.4	0.2	7.2	0.1	2425	2081	7
925-33	35.8	0.2	0.0	2.8	0.2	8.0	0.1	2435	2061	24
925-34	35.9	0.2	0.0	2.6	0.4	6.9	0.2	2427	2065	19
925-35	36.0	0.1	0.0	1.3	0.2	3.8	0.1	2429	2073	—
925-35-28m	35.9	0.1	0.0	1.5	0.2	4.1	0.1	—	2069	—
925-36	35.3	0.0	0.0	—	—	—	—	2430	2067	—
925-37	34.8	0.0	0.0	1.1	0.1	1.1	0.1	2429	2054	—
925-38	34.6	0.0	0.0	1.1	0.2	1.3	0.1	2442	2065	26
925-39	35.0	0.0	0.0	1.0	0.1	1.2	0.0	2436	2057	43
925-40	35.7	0.0	0.0	0.6	0.1	1.4	0.0	2432	2048	—
925-41	35.6	0.0	0.0	3.9	0.2	12.9	0.1	2440	2060	76
925-42	35.8	0.1	0.0	1.3	0.2	3.3	0.1	2429	2069	2
925-43	35.8	0.1	—	2.0	0.2	5.5	0.1	—	2080	32
925-44	35.8	0.1	—	2.3	0.2	6.0	0.1	2429	2062	27
925-45	35.4	0.3	0.0	1.0	0.2	4.2	0.1	2431	2036	—
925-46	35.6	0.4	0.0	3.5	0.2	8.6	0.1	2425	2065	20
925-47	35.7	0.3	0.0	3.6	0.3	8.9	0.2	2437	2102	24
925-48	35.8	1.4	0.2	5.6	0.7	15.5	0.4	2438	2131	8
925-49	34.6	0.6	0.1	5.1	0.2	11.4	0.1	2587	2259	21
925-50	34.1	1.6	0.3	5.6	0.2	1.3	0.1	2582	2287	—
925-51	33.6	1.3	0.2	6.8	0.5	17.5	0.3	2599	2308	13
925-52	30.4	3.4	0.6	10.9	0.6	20.8	0.3	2352	2063	6
925-53	35.0	0.1	0.0	2.6	0.3	6.3	0.2	2445	2004	32
925-54	35.5	0.3	0.0	3.6	0.3	8.0	0.2	—	—	24
925-55	35.5	0.0	0.0	1.0	0.1	2.0	0.0	2449	—	—

Table 1. Continued.

Station	Salinity	^{223}Ra (Bq m^{-3})	ex ^{224}Ra (Bq m^{-3})	^{228}Ra (Bq m^{-3})	± (Bq m^{-3})	^{226}Ra (Bq m^{-3})	± (Bq m^{-3})	TAlk (μmol L^{-1})	DIC (μmol L^{-1})	Water age (d)
925-56	35.7	0.5	0.1	3.3	0.3	8.8	0.2	2425	—	13
925-57	36.3	0.1	0.0	1.9	0.1	5.7	0.1	2430	—	21
925-58	36.0	0.3	0.0	4.1	0.1	14.0	0.1	2491	2108	28
925-59	36.1	0.2	0.0	4.0	0.3	14.6	0.2	2497	2115	31
925-60	35.7	0.5	0.0	4.5	0.1	13.7	0.1	2537	2140	21
925-60-11m	35.6	0.6	0.1	4.7	0.3	15.1	0.2	—	2141	—
925-61	35.6	0.5	0.0	4.7	0.1	13.6	0.2	2567	2183	21
925-62	35.1	1.0	0.2	7.8	0.1	18.6	0.2	2586	2281	21
925-63	35.9	0.3	0.0	4.0	0.3	12.5	0.5	2453	—	29
925-64	36.2	0.1	0.0	1.7	0.1	6.2	0.1	2405	2060	18
925-64-19m	36.3	0.2	0.0	1.5	0.2	6.1	0.2	—	2072	—
925-65	35.7	0.5	0.1	7.2	0.4	15.2	0.3	2531	2179	29
925-66	36.7	0.5	0.1	5.3	0.4	13.3	0.3	2489	2099	23
925-67	36.5	0.2	0.0	3.7	0.7	10.7	0.2	2473	2093	31
925-68	36.5	0.1	0.0	1.2	0.2	5.1	0.2	2452	2139	—
925-69	36.9	0.1	0.0	2.5	0.2	8.1	0.1	2430	2077	32
925-69-12m	36.8	0.2	0.0	2.6	0.6	8.3	0.2	—	—	—
Tampa Bay										
925-17	24.9	4.8	7.2	14.9	0.6	26.5	0.3	2294	2054	—
925-18	27.8	3.6	5.9	15.0	0.7	25.9	0.3	2294	2060	—
925-19	30.1	1.7	2.4	11.7	0.5	19.9	0.3	2348	2093	—
925-20	32.5	2.3	4.0	8.4	0.8	13.1	0.4	2395	2088	—
925-21	34.8	0.8	0.1	5.8	0.5	9.8	0.3	2442	—	17
925-22	35.4	0.6	0.0	4.0	0.2	7.0	0.1	2436	2075	14
Charlotte Harbor										
2	25.7	1.5	2.6	9.4	1.2	17.4	0.7	2287	2029	—
4	22.5	8.1	10.5	14.4	0.8	26.2	0.4	2199	1873	—
6	20.2	5.4	4.5	12.5	1.2	22.8	0.6	2150	1900	—
8	12.8	4.3	3.3	10.2	1.3	19.5	0.7	1890	1864	—
10	0.2	0.3	1.1	2.2	0.8	10.2	0.4	1446	1525	—
925-52	30.4	3.4	0.6	10.9	0.6	20.8	0.3	2352	2063	6
Caloosahatchee River estuary										
C1	6.3	1.7	1.5	4.6	0.5	40.4	0.5	2788	2762	—
C2	2.2	0.6	0.5	2.0	0.3	24.1	0.3	2966	3004	—
C3	0.5	0.3	0.5	1.7	0.4	22.7	0.4	2933	3020	—
C4	0.3	0.4	0.5	1.7	0.3	20.2	0.3	2978	3150	—
C5	32.5	4.8	2.8	6.3	0.5	17.5	0.3	2621	2350	—
C6	33.2	4.9	2.7	7.7	0.6	21.9	0.4	2616	2389	—
C8	16.5	3.1	2.4	5.5	0.5	27.4	0.4	2650	2572	—
C9	12.0	1.7	1.4	4.6	0.5	29.1	0.4	2702	2665	—
C10	8.8	1.6	1.6	4.1	0.5	33.4	0.4	2727	2707	—
C10B	5.2	1.5	1.3	3.3	0.4	32.4	0.4	2776	2658	—
C10C	0.4	0.5	0.6	2.0	0.5	31.4	0.5	3058	3224	—
C11	0.3	0.7	0.8	1.7	0.6	31.2	0.5	3281	3097	—
C12	0.2	0.7	0.4	2.2	0.5	27.3	0.5	3341	3491	—
C13	0.1	0.6	0.1	2.1	0.5	4.8	0.2	1120	779	—

* Water column samples were collected at Sta. 902-28, 902-32, 902-33, 902-39, 902-42, 902-44, 902-49, 925-35, 925-60, 925-64, and 925-69; only surface water was collected at the rest of the stations.

pore water collected by piezometers ranged from 7.6 to 27.3. Groundwater along the CRE was highly enriched in ^{226}Ra, with minimal variability between seasons (Fig. 5a; Table 2). Radium-226 ranged from 8.3–575 Bq m^{-3} (median 45 Bq m^{-3}) in the low-salinity groundwater and 18.3–3758 Bq m^{-3} (median 183 Bq m^{-3}) in the high-salinity groundwater (Fig. 5a; Table 2). CRE groundwater had a relatively low average ^{228}Ra : ^{226}Ra ratio (0.2) due to the presence of phosphorite deposits, which contain elevated activities of uranium and its decay products (Charette et al. 2013). High-salinity CRE groundwater had higher ^{228}Ra relative to low-salinity groundwater, with average ^{228}Ra of 91 Bq m^{-3} and 8 Bq m^{-3}, respectively. No significant difference in CRE groundwater ^{226}Ra and ^{228}Ra was observed as compared to other groundwater along the shoreline of SWFS (Table 2). These groundwater sampling locations include Tampa Bay, Everglades, Key Largo, Loxahatchee River estuary; taken together, the average

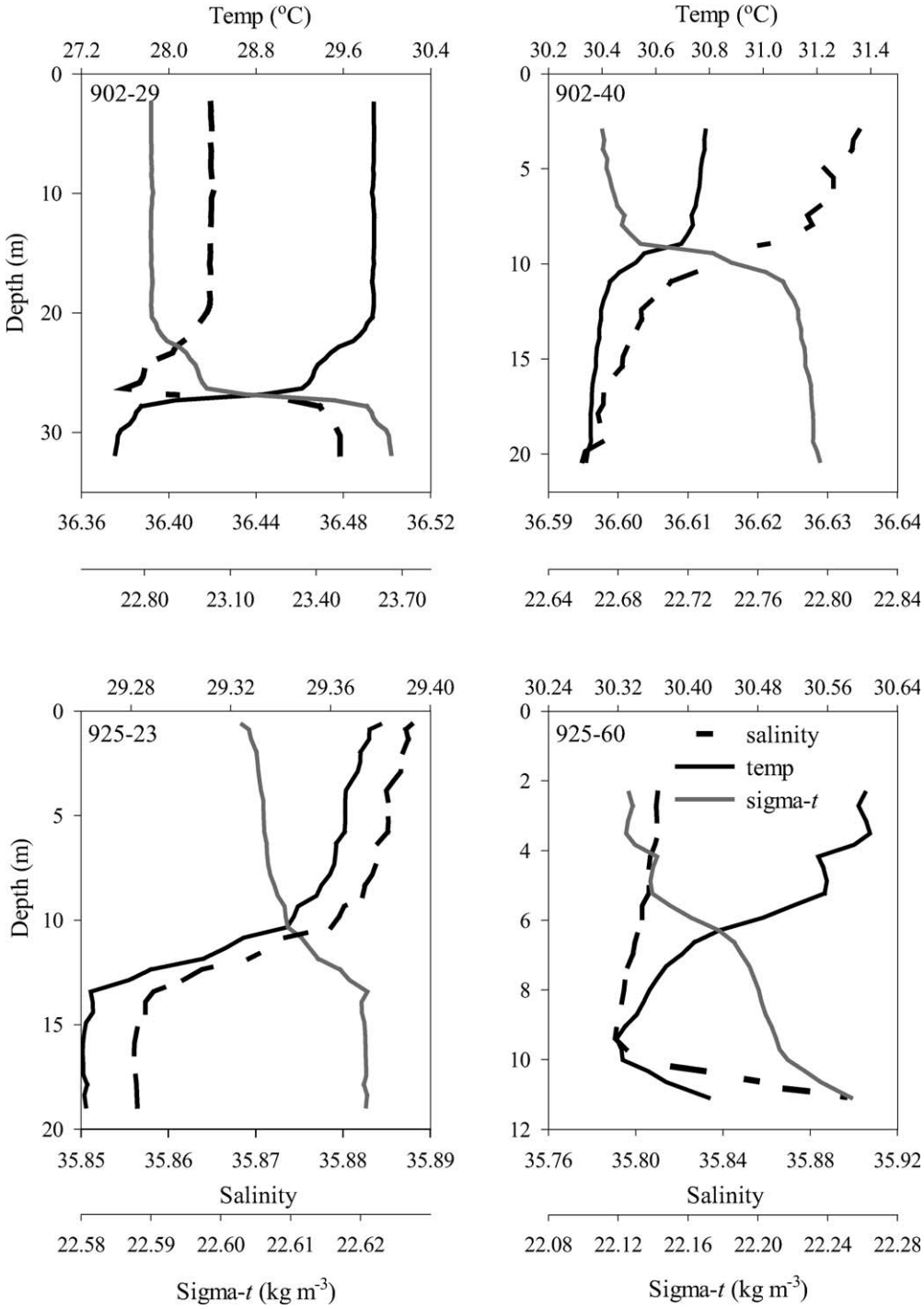

Fig. 4. Vertical profiles of salinity, temperature (temp, °C), and sigma-*t* (density − 1000, kg m^{-3}) at sites 902-29 and 902-40 in July 2009 and sites 925-23 and 925-60 in October 2009. Station locations are shown in Fig. 2.

^{226}Ra and ^{228}Ra of all the groundwater near the coast of SWFS was 183 ± 500 and 27 ± 70 Bq m^{-3}, respectively. The error bars are 1 standard deviation (SD) of the average, and provide an estimate of the spatial variation of radium in the groundwater.

Ra activity in the estuaries: In July, ^{226}Ra and ^{228}Ra ranged from 5.4 to 32.5 Bq m^{-3} and 1.8 to 15.6 Bq m^{-3}, respectively, over a salinity range of 0.2–33.2 in the SRE (Table 1; Fig. 5b). In October, ^{226}Ra ranged from 13.1–26.5 Bq m^{-3}, and ^{228}Ra ranged from 4.0–15.0 Bq m^{-3} over a salinity range of 24.9–32.5 in Tampa Bay, from 10.2–26.2 Bq m^{-3} for ^{226}Ra and 2.2–14.4 Bq m^{-3} for ^{228}Ra for salinities ranging from 0.2–25.7 in Charlotte Harbor, and from 4.7–40.3 Bq m^{-3} for ^{226}Ra and 1.7–7.7 Bq m^{-3} for

^{228}Ra over a salinity range of 0.1–32.5 in the CRE. Total particulate ^{226}Ra (> 1 μm) in the freshwater reaches of the CRE was 0.3 Bq m^{-3}. While each estuary had a different ^{226}Ra range, the ^{226}Ra distribution was similar: ^{226}Ra increased with salinity (S) until reaching a peak at intermediate salinity, then decreased upon further mixing with a lower ^{226}Ra seawater end-member (Fig. 5b). We can obtain the effective riverine ^{226}Ra activity (^{226}Ra at S = 0) by extrapolating back to S = 0 from the linear relationship between salinity and ^{226}Ra at S values above the Ra peak. This approach has been discussed in Officer (1979). Radium-228 showed a similar trend to ^{226}Ra in the SRE, Tampa Bay, and Charlotte Harbor, with the one exception being the CRE, where ^{228}Ra in the seawater end-member was greater than the riverine activity (figure not shown). The detailed spatial and temporal distributions of radium activities in the CRE were presented in Charette et al. (2013).

Ra in the shelf water: Shelf-water Ra isotope distributions were similar in July and October. Both short-lived and long-lived Ra isotopes were enriched in the nearshore water, consistent with sources from rivers (dissolved and desorption from suspended particles), SGD, and diffusion from sediments into the water column. Moving seaward from the inner shelf, Ra activities decreased gradually to the outer shelf with little spatial variation in the offshore water (> 100 km offshore; Fig. 6a,b). Radium-226,^{228}Ra, ^{223}Ra, and excess ^{224}Ra ranged from 1.1–25.9, 0.7–14.3, 0–4.4, and 0.1–7.8 Bq m^{-3} (Table 1), respectively; the upper end of the ^{226}Ra range is one order of magnitude lower than the average groundwater activity. The ^{226}Ra values in the SWFS (average = 8.4 Bq m^{-3}) are among the highest ever reported for an open shelf system—for comparison, in the seminal study of Moore (1996) on SGD in the South Atlantic Bight, ^{226}Ra only ranged from 1.3–4.6 Bq m^{-3}. In the offshore seawater with relatively low salinity, Ra activities approached the background activity of ~ 1.3 Bq m^{-3} (Boyle et al. 1984; Fig. 7a,b), suggesting little Ra contribution to our study domain from northern Gulf of Mexico river plumes. Surface-water Ra activities showed no statistical difference between July and October (Fig. 5c). Ra-226 activities decreased with increasing salinity for these two seasons over the shelf; most of the samples fell between conservative mixing lines of river–seawater and groundwater–seawater (Fig. 5c), indicating three end-member mixing from river, groundwater, and offshore seawater. The few samples that fall beyond these two mixing lines may be due to the uncertainty in the mixing lines from very limited estuarine data and a wide range of radium activities in the groundwater. The river flux–weighted average ^{226}Ra at zero salinity (Ra_r) was calculated as:

$$Ra_r = \sum_{i=1}^{3} (Q^i_{RIV} \times Ra_i) / \sum_{i=1}^{3} Q^i_{RIV} \quad (1)$$

where i represents the number of estuaries, including Charlotte Harbor, CRE, and SRE, Q^i_{RIV} is the river flux in each estuary obtained from the respective gauging station, and Ra_i is the effective riverine ^{226}Ra for each estuary.

Bottom-water ^{226}Ra and ^{228}Ra activities were close to or slightly higher than surface water at stations with stratification, and they were identical in stations with a well-mixed water column (Table 1). Two exceptions existed near an offshore sinkhole (Site 902-42) and at the geothermal spring seepage zone (Site 925-60; Mud Hole Spring). At the sinkhole, bottom water had lower ^{226}Ra and ^{228}Ra compared with the surface water (8.3 vs. 11.3 Bq m^{-3} for ^{226}Ra; 2.8 vs. 3.6 Bq m^{-3} for ^{228}Ra). In contrast, at the hydrothermal spring, ^{226}Ra in the bottom water was slightly higher than that in the surface water (15.1 vs. 13.7 Bq m^{-3}), while ^{228}Ra was similar (4.7 vs. 4.5 Bq m^{-3}). However, the volumetric spring contribution at this station must have been relatively small, assuming a ^{226}Ra activity for Mud Hole Spring of 1717 Bq m^{-3} (Fanning et al. 1981).

TAlk and DIC distribution in the groundwater, estuaries, and shelf water—TAlk and DIC patterns in the groundwater: Relative to surface-water sources, groundwater had high concentrations of TAlk and DIC. TAlk ranged from 2375–9595 μmol L^{-1} (Table 2; Fig. 8a), with an average of 5106 μmol L^{-1}, while DIC ranged from 3332–11,607 μmol L^{-1} (Table 2; Fig. 8b), with an average of 5804 μmol L^{-1}. There were no significant differences between seasons and years. In terrestrial groundwater (salinity range: 0–1.5), the TAlk concentration was between 2375 and 9595 μmol L^{-1} (averaging 5371 μmol L^{-1}) and DIC was between 3754 and 11,607 μmol L^{-1} (averaging 6175 μmol L^{-1}). Marine groundwater (salinity range: 2–40) had TAlk concentrations spanning 3129 and 8374 μmol L^{-1} (averaging 4578 μmol L^{-1}) and a DIC range of 3332–8905 μmol L^{-1} (averaging 5227 μmol L^{-1}). There was no statistical difference between TAlk and DIC in terrestrial vs. marine groundwater.

TAlk and DIC patterns in the estuaries: In the CRE, TAlk and DIC were negatively correlated with salinity at salinities > 6 (TAlk = −5S + 2787, R^2 = 0.86, n = 8; DIC = −13S + 2798, R^2 = 0.95, n = 8). Positive correlations between TAlk and salinity, and DIC and salinity were observed in Charlotte Harbor (TAlk = 29S + 1502, R^2 = 0.97, n = 7; DIC = 16S + 1568, R^2 = 0.93, n = 7) and Tampa Bay (TAlk = 16S + 1881, R^2 = 0.94, n = 5; DIC = 5S + 1918, R^2 = 0.77, n = 4) in October 2009 (Table 1; Fig. 8c,d). The SRE (July 2009) had higher concentrations of TAlk and DIC than the other local estuaries: TAlk and DIC ranged from 2534 to 3418 μmol L^{-1} and 2306 to 4016 μmol L^{-1}, respectively (Table 1; Fig. 8c,d). We only had eight stations in the SRE, and while salinities were close to zero in four of them, we found a negative correlation for the higher salinities vs. TAlk and DIC (TAlk = −29S + 3778, R^2 = 0.88, n = 4; DIC = −58S + 4805, R^2 = 0.72, n = 4). Charlotte Harbor had the lowest TAlk and DIC of the four estuaries.

TAlk and DIC patterns in the shelf water: Similar to Ra, there were no apparent seasonal variations of TAlk and DIC on the SWFS. TAlk concentrations ranged from 2234–2787 μmol L^{-1}, while DIC ranged from 1908–2473 μmol L^{-1} (Table 1; Fig. 8e,f). Both TAlk and DIC were enriched in nearshore water, which might reflect a combination of

Table 2. Measurements of ^{226}Ra, total alkalinity (TAlk), and dissolved inorganic carbon (DIC) in groundwater samples in southwest Florida. The sampling sites near the Caloosahatchee River estuary were shown in Fig. 1b. Dashes indicate no data.

Site	Date	Salinity	^{226}Ra (Bq m^{-3})	^{228}Ra (Bq m^{-3})	TAlk (μmol L^{-1})	DIC (μmol L^{-1})
Caloosahatchee River estuary*						
GW1	13 Apr 09	0.3	8	2	—	5970
	12 Oct 09	0.4	17	2	6612	7810
GW2	13 Apr 09	40.0	400	47	2967	6038
	12 Oct 09	32.9	148	42	7849	8421
	15 Apr 10	32.4	183	50	6533	6559
	20 Oct 10	40.2	167	5	—	—
GW3	13 Apr 09	0.4	72	5	3938	4047
	12 Oct 09	5.4	22	15	9595	11,607
	14 Apr 10	0.3	73	7	3725	3754
	17 Oct 10	0.2	55	5	—	—
GW4	13 Apr 09	0.4	52	10	—	6959
	12 Oct 09	0.3	42	7	5707	6782
GW5	13 Apr 09	1.5	122	15	—	8246
	12 Oct 09	2.5	27	31	8374	8905
	13 Apr 10	2.8	183	25	7686	8114
	17 Oct 10	2.6	217	30	—	—
GW6	13 Apr 09	1.2	367	15	—	5432
	12 Oct 09	0.8	267	14	4344	6106
	14 Apr 10	1.0	383	16	5109	5900
	17 Oct 10	1.0	317	15	—	—
GW7	13 Apr 09	0.3	15	3	—	6454
	13 Oct 09	0.3	25	4	6063	7096
GW8	14 Apr 09	0.6	25	2	6413	6996
	13 Oct 09	0.7	63	8	6204	6989
GW9	14 Apr 09	0.4	255	7	—	7812
	13 Oct 09	0.4	239	6	6723	7974
	15 Apr 10	0.4	190	5	7105	8458
GW10	14 Apr 09	0.4	27	5	4879	5753
	13 Oct 09	0.6	32	4	6679	8207
	15 Apr 10	0.6	16	2	7794	9460
	19 Oct 10	0.6	28	8	—	—
GW13	14 Apr 09	0.4	43	4	3991	3854
	12 Oct 09	0.4	51	4	3959	3847
	13 Apr 10	0.4	52	6	4150	3954
	17 Oct 10	0.4	64	5	—	—
GW14	15 Apr 09	3.6	574	8	3129	3361
	14 Oct 09	2.1	151	12	4111	4067
GW15	15 Apr 09	2.3	202	13	3976	3978
	14 Oct 09	3.5	455	6	3214	3403
GW16	15 Apr 09	0.8	57	16	6064	7274
	14 Oct 09	0.9	43	16	7040	8686
GW17	15 Apr 09	0.4	24	22	—	4445
	14 Oct 09	0.4	21	20	2375	3963
GW18	15 Apr 09	0.2	39	3	4018	4274
	13 Oct 09	0.2	46	5	4125	4603
CAL212	14 Apr 10	20.4	1658	150	—	8142
CAL213	14 Apr 10	17.0	1422	213	—	5022
CAL313	20 Oct 10	18.4	976	89	—	—
CAL214	14 Apr 10	17.6	374	77	4070	4218
CAL314	20 Oct 10	27.3	3758	494	—	—
CAL215	14 Apr 10	8.3	19	5	3201	3332
CAL315	20 Oct 10	15.4	672	64	—	—
CAL216	14 Apr 10	7.6	25	6	3749	3495
	20 Oct 10	13.3	38	9	—	—
CAL317	20 Oct 10	8.0	31	9	—	—
Tampa Bay†						
GW01	2005	2.6	48	20	—	—
GW02	2005	19.0	58	28	—	—
GW03	2005	11.3	45	22	—	—

Table 2. Continued.

Site	Date	Salinity	^{226}Ra (Bq m^{-3})	^{228}Ra (Bq m^{-3})	TAlk (μmol L^{-1})	DIC (μmol L^{-1})
Loxahatchee River estuary‡						
Well1	15 Sep 03	0.3	18	10	—	—
	08 Mar 04	0.2	15	7	—	—
Well3	16 Sep 03	0.1	15	10	—	—
	09 Mar 04	0.1	87	25	—	—
Well7	08 Mar 04	0.0	5	7	—	—
	15 Sep 03	0.0	8	bd	—	—
Everglades§						
MBseawrd	03 Mar 94	—	214	92	—	—
MBinshor	03 Mar 94	—	217	93	—	—
3059802	04 Mar 94	—	15	3	—	—
3059803	04 Mar 94	—	18	2	—	—
3059804	04 Mar 94	—	20	5	—	—
3059805	04 Mar 94	—	19	4	—	—
3059806	04 Mar 94	—	10	1	—	—
MP1-A	08 Sep 93	—	22	4	—	—
MP1-D	08 Sep 93	—	12	1	—	—
U3-GW3	10 Sep 93	—	171	1	—	—
U3-SW	10 Sep 93	—	24	3	—	—
F1-GW3	13 Sep 93	—	177	6	—	—
F1-GW4	13 Sep 93	—	10	2	—	—
F1-SW	13 Sep 93	—	18	2	—	—
S10C-TW	13 Sep 93	—	18	3	—	—
MP3-A	14 Sep 93	—	171	42	—	—
MP3-D	14 Sep 93	—	45	3	—	—
ENR002	15 Sep 93	—	26	4	—	—
ENR004	15 Sep 93	—	20	3	—	—
Key Largo‖						
KL-1	03 Nov 93	—	56	8	—	—
KL-2	23 Oct 93	—	82	0	—	—
KL-3	23 Oct 93	—	195	0	—	—
KL-4	23 Oct 93	—	77	0	—	—
KL-5	27 Oct 93	—	52	0	—	—
OR-1A	03 Nov 93	—	150	12	—	—
OR-1B	03 Nov 93	—	44	7	—	—
OR-3	24 Oct 93	—	66	0	—	—
OR-4	24 Oct 93	—	260	0	—	—
OR-5	24 Oct 93	—	19	2	—	—
BS-A	03 Nov 93	—	184	39	—	—
BS-B	03 Nov 93	—	65	2	—	—
FL37	09 Sep 03	32.4	42	7	—	—
FL51	10 Sep 03	35.8	13	2	—	—
Submarine Spring¶						
MHSS	1978–1980	34.9	1723	≥85	—	—
Spring III	13 Jun 79	35.0	≥897	—	—	—
Spring V	16 Jun 79	35.1	1382	80	—	—

bd denotes below detection.
* Site GW denotes monitoring wells, CAL represents pore water collected along the Caloosahatchee River estuary.
† Swarzenski et al. (2007).
‡ Swarzenski et al. (2006).
§ Paytan unpubl. data.
‖ Moore et al. (2008).
¶ Fanning et al. (1981).

sources including rivers, SGD, as well as sediment release; concentrations decreased upon mixing with seawater farther offshore until reaching background Gulf of Mexico levels (Figs. 6c,d; 7c,d). As with ^{226}Ra, a simple river–seawater mixing line cannot explain the TAlk and DIC patterns on the shelf. Most of the samples fall on the groundwater–seawater mixing line, suggesting a quantitatively important TAlk and DIC contribution from SGD (Fig. 8e,f). The TAlk and DIC end-members for the estuaries were estimated using the same approach as for Ra_r in Eq.1.

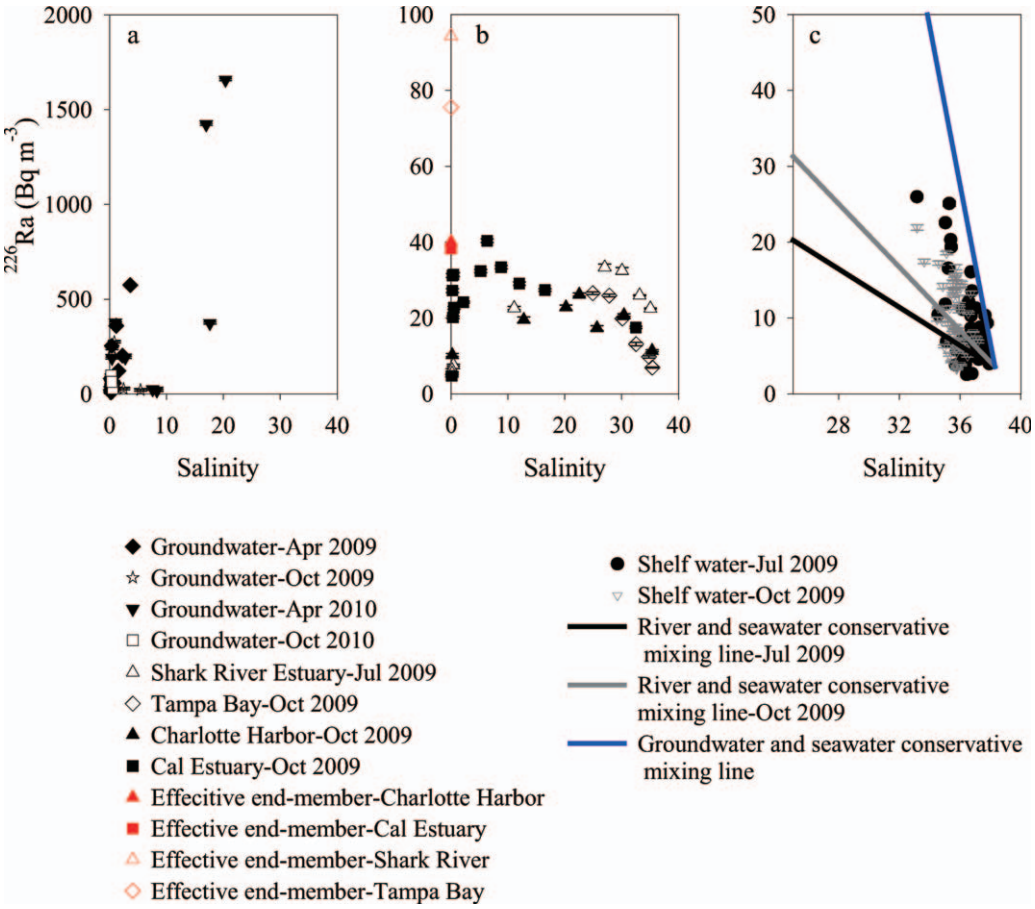

Fig. 5. Radium-226 vs. salinity for (a) groundwater (April and October in both 2009 and 2010) along the Caloosahatchee River estuary (CRE), (b) estuaries, and (c) surface water (July and October 2009) on the southwest Florida Shelf. The estuaries include Shark River (July 2009), Tampa Bay (October 2009), Charlotte Harbor (October 2009), and CRE (October 2009). Error bars are based on counting statistics. (c) Most of the shelf samples fall between conservative mixing lines of river–seawater and groundwater–seawater, indicating three end-members mixing from river, groundwater, and offshore seawater. The ^{226}Ra (Bq m^{-3}) relationship with salinity in the estuaries (at salinity values above the Ra peak) was as follows: Ra = $-0.8S + 40$, $R^2 = 0.67$, $n = 5$ for Charlotte Harbor in October; Ra = $-0.6S + 38$, $R^2 = 0.83$, $n = 7$ for Caloosahatchee River estuary in October; Ra = $-3.5S + 140$, $R^2 = 0.94$, $n = 3$ for Shark River estuary in July; Ra = $-2.4S + 92$, $R^2 = 0.99$, $n = 5$ for Tampa Bay in October. (b) The respective effective ^{226}Ra end-member in each estuary is displayed.

Discussion

In this section, we employ two approaches to assess the effect of SGD on the SWFS inorganic carbon budget. We performed a ^{226}Ra mass balance for the SWFS in which shelf-water exchange rates (water ages) are estimated from ^{223}Ra : ^{228}Ra ratios, and are used to estimate the role of SGD in the ^{226}Ra budget. This ^{226}Ra budget and the observed ^{226}Ra activity in groundwater are then used to estimate the volumetric flux of SGD. This SGD water flux estimate is combined with the groundwater TAlk and DIC concentrations to estimate the SGD-associated TAlk and DIC fluxes. We also estimated the TAlk and DIC fluxes from the SGD ^{226}Ra flux and the ^{226}Ra : DIC and TAlk : ^{226}Ra relationships in the shelf water. For comparison, we utilize data from our study and the literature to construct budgets of TAlk and DIC on the SWFS, and to quantify the relative role of SGD in these budgets. We then compare these estimates with our direct (^{226}Ra-based) estimates of the SGD fluxes of TAlk and DIC.

SGD flux derived from ^{226}Ra mass balance—Ra-226 was enriched in the groundwater relative to the estuaries and shelf water (Fig. 5). To quantify the SGD input, we constructed a steady-state radium mass balance model for the SWFS (Eq. 2). Besides SGD, model Ra sources include total river input (dissolved ^{226}Ra and ^{226}Ra desorption from suspended particles), diffusion from shelf sediments, and hydrothermal submarine springs. The only Ra sink is mixing with offshore seawater. Radioactive decay can be ignored due to the long half-life of ^{226}Ra. Alongshore transport may be a source or sink to the study domain depending on the current direction and any Ra activity differences between the two boundary transects in the north and south of the box model. The West Florida Continental Shelf mean flow is oriented approximately along-isobath and southward (Weisberg et al. 2009). To maintain

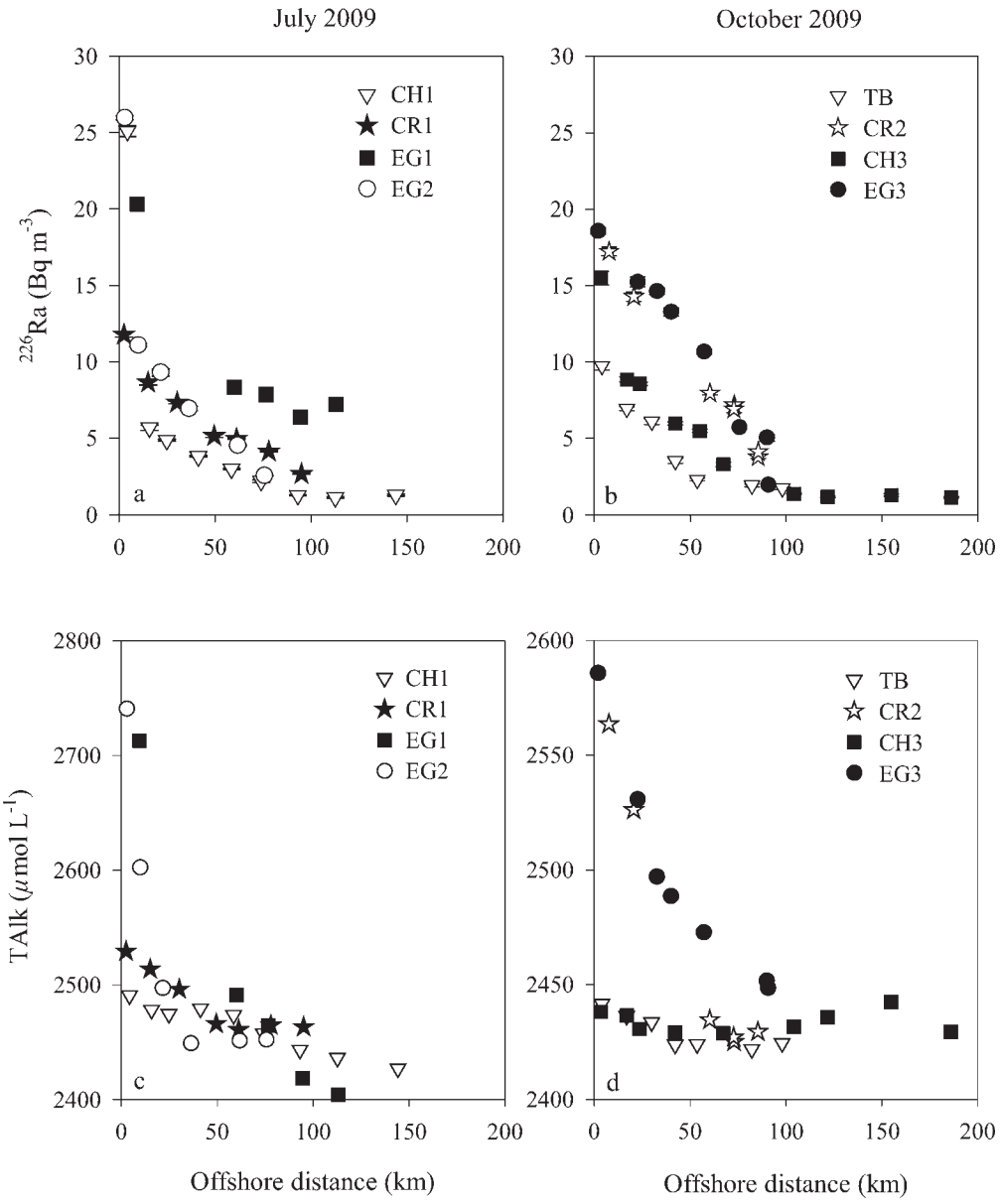

Fig. 6. Radium-226 and total alkalinity (TAlk) distributions plotted against distance in the surface water of southwest Florida Shelf during (a, c) July 2009 and (b, d) October 2009.

consistent alongshore current rates between our transects, we set up a box model that encompasses the 40 m isobath, or ~ 80 km offshore (Fig. 1a). To compare the SGD flux covering the same area in July and October, the box was divided into two parts with and without the TB Transect, which was only conducted in October (gray line in Fig. 1a). The mass balance model is written as follows:

$$\frac{^{226}\mathrm{Ra}^{\mathrm{inv}}}{\tau} = \left(\sum [\mathrm{Q_{RIV}} \times {}^{226}\mathrm{Ra}^{\mathrm{act}}_{\mathrm{RIV}}]\right) + \left(\mathrm{A_{SED}} \times {}^{226}\mathrm{Ra}^{\mathrm{flux}}_{\mathrm{SED}}\right) + \left(\mathrm{Q_{HS}} \times {}^{226}\mathrm{Ra}^{\mathrm{act}}_{\mathrm{HS}}\right) + \left(\mathrm{Q_{SGD}} \times {}^{226}\mathrm{Ra}^{\mathrm{act}}_{\mathrm{SGD}}\right) \pm \left(\mathrm{Q_A} \times \left(\Delta^{226}\mathrm{Ra}^{\mathrm{act}}_{\mathrm{A}}\right)\right) \quad (2)$$

where the left-hand side represents the ^{226}Ra flux exchange with offshore seawater, $^{226}\mathrm{Ra}^{\mathrm{inv}}$ is the excess ^{226}Ra inventory in the shelf system (where the excess is determined by subtracting the offshore ^{226}Ra activity), τ is the water age (estimated using ^{223}Ra and ^{228}Ra data, as discussed below); the right-hand terms denote ^{226}Ra inputs from local rivers ($\sum [\mathrm{Q_{RIV}} \times {}^{226}\mathrm{Ra}^{\mathrm{act}}_{\mathrm{RIV}}]$), sediment release ($\mathrm{A_{SED}} \times {}^{226}\mathrm{Ra}^{\mathrm{flux}}_{\mathrm{SED}}$), nearshore hydrothermal springs ($\mathrm{Q_{HS}} \times {}^{226}\mathrm{Ra}^{\mathrm{act}}_{\mathrm{HS}}$), SGD along the shoreline ($\mathrm{Q_{SGD}} \times {}^{226}\mathrm{Ra}^{\mathrm{act}}_{\mathrm{SGD}}$), and alongshore transport (source or sink, $\pm \mathrm{Q_A} \times (\Delta^{226}\mathrm{Ra}^{\mathrm{act}}_{\mathrm{A}})$). The detailed information for each item is presented in Table 3. Unlike ^{226}Ra, ^{228}Ra activities in most groundwater samples were of the same magnitude as estuaries and shelf water; hence, we only used a ^{226}Ra mass balance model to the calculate SGD flux.

Apparent water ages determined by ^{223}Ra: ^{228}Ra: A key term in the radium mass balance presented in Eq. 2 is Ra

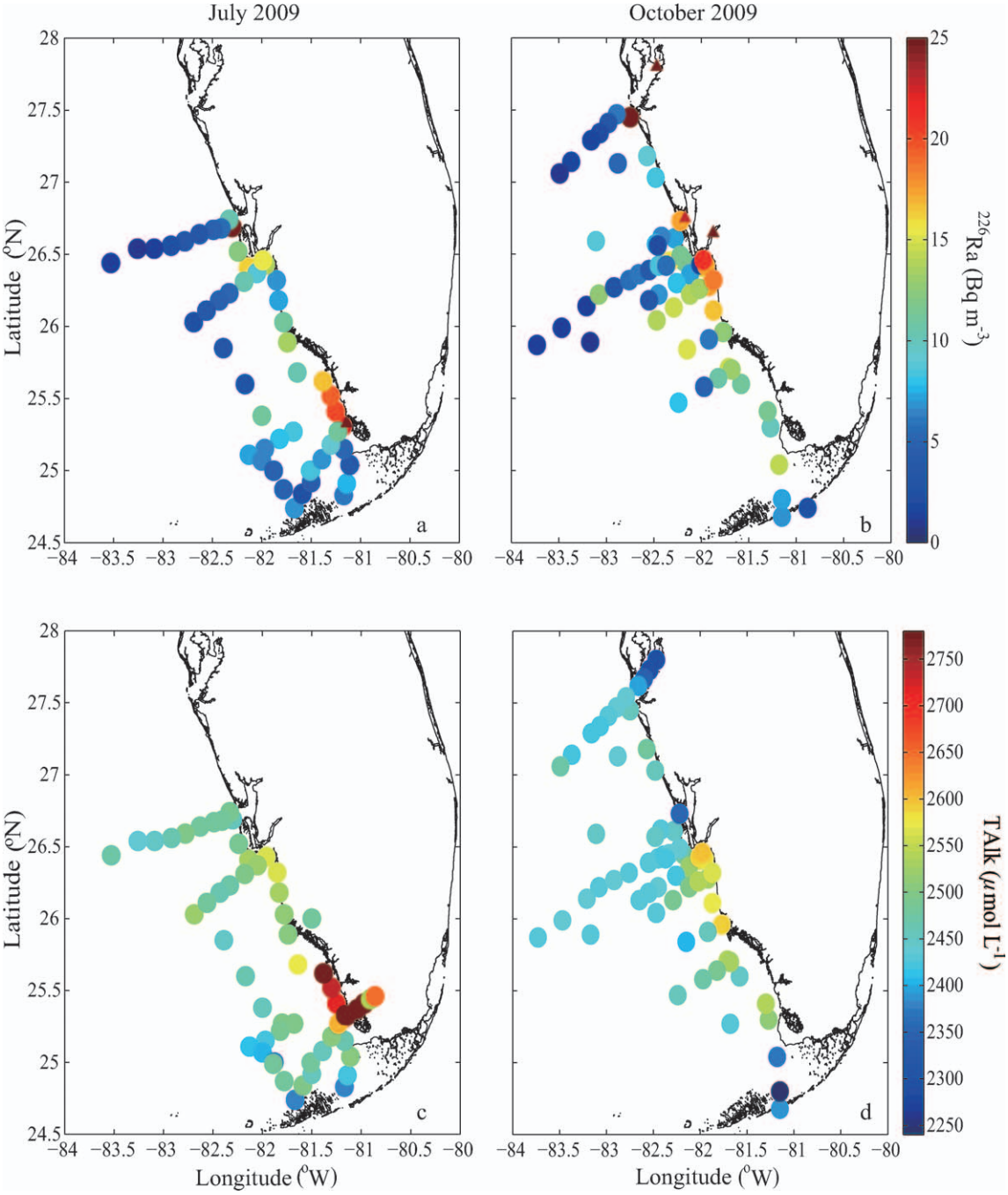

Fig. 7. Radium-226, total alkalinity (TAlk) distributions in the surface water of southwest Florida Shelf during (a, c) July 2009 and (b, d) October 2009. (a, b) The triangle denotes the location of ^{226}Ra peak in each estuary.

exchange from mixing between the SWFS and the Gulf of Mexico; for this we require the mean water age of our model "box." Ra isotope activity ratios (ARs) have been used to estimate apparent water age, defined as the time elapsed since a water parcel is initially enriched in the Ra isotopes without further Ra addition (Moore 2000). Ra distributions in shelf water are mainly controlled by mixing and radioactive decay. If the Ra AR of the source is constant along the coast, then the Ra AR is independent of mixing effects, making the Ra AR distribution in the shelf water a function of the decay constant for the two Ra isotopes. Given that the short half-life of ^{224}Ra ($T_{1/2}$ = 3.7 d) might not be appropriate for assessing the water age in continental shelf waters, we used ^{223}Ra : ^{228}Ra to estimate water age. The mathematical equation was as follows (Moore 2000; Charette et al. 2001):

$$\left[\frac{ex^{223}\mathrm{Ra}}{ex^{228}\mathrm{Ra}}\right]_{\mathrm{obs}} = \left[\frac{ex^{223}\mathrm{Ra}}{ex^{228}\mathrm{Ra}}\right]_{\mathrm{i}} e^{-\lambda_{223}\tau} \quad (3)$$

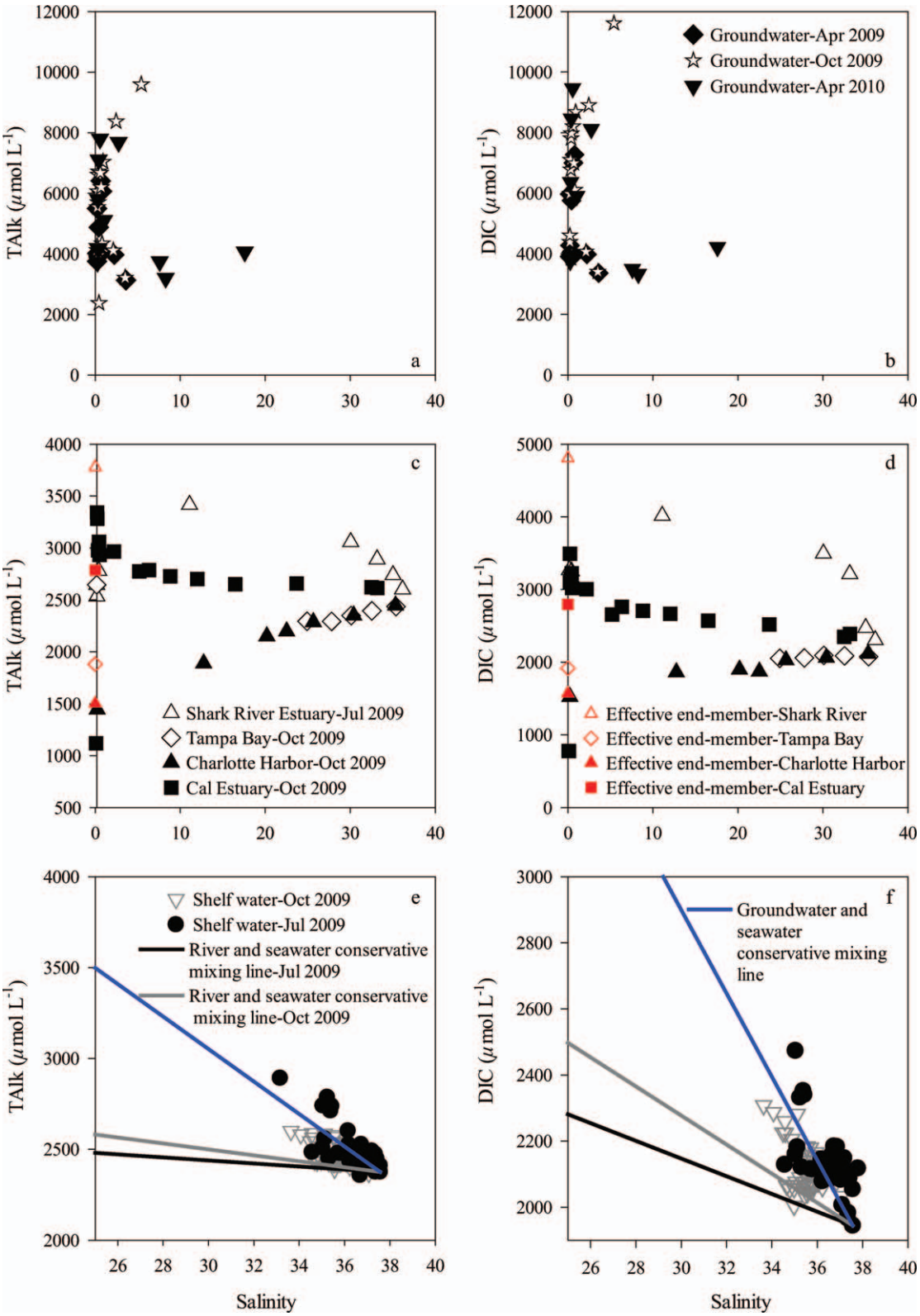

Fig. 8. Total alkalinity (TAlk) vs. salinity and dissolved inorganic carbon (DIC) vs. salinity for (a, b) groundwater along the Caloosahatchee River estuary (CRE), (c, d) estuaries, and (e, f) surface water on the southwest Florida Shelf. The estuaries include Shark River (July 2009), Tampa Bay (October 2009), Charlotte Harbor (October 2009), and CRE (October 2009). (e, f) Black and gray lines denote the expected concentrations of TAlk and DIC from conservative mixing between river water and offshore seawater, and the blue line is conservative mixing of groundwater and seawater. Most of the shelf samples fall on the groundwater–seawater mixing line, suggesting a quantitatively important TAlk and DIC contribution from SGD.

Table 3. Definitions and values used for ^{226}Ra (Eq. 2), total alkalinity (TAlk, Eq. 7), and dissolved inorganic carbon (DIC, Eq. 8) mass balances to estimate submarine groundwater discharge and associated TAlk and DIC fluxes to the southwest Florida Shelf in July and October 2009.

	Definition	July	October	Units	Reference
$^{226}Ra^{inv}$	Excess ^{226}Ra inventory in the shelf system	1.08×10^{12}	1.04×10^{12}	Bq	this study
τ	Average water age	28	30	days	this study
Q_{RIV}	Discharge of rivers	*see* Table 5		$m^3\ d^{-1}$	USGS* data
$^{226}Ra^{act}_{RIV}$	Ra end-member in the estuaries	*see* Table 5		Bq m^{-3}	this study
A_{SED}	Study area	1.38×10^{10}		m^2	this study
$^{226}Ra^{flux}_{SED}$	Diffusion flux of Ra from sediments	0.02		Bq $m^{-2}\ d^{-1}$	Miller et al. 1990
Q_{HS}	Hydrothermal spring rate	2160		$m^3\ d^{-1}$	Fanning et al. 1981
$^{226}Ra^{act}_{HS}$	Ra activity in the hydrothermal spring	1717		Bq m^{-3}	Fanning et al. 1981
$^{226}Ra^{act}_{SGD}$	Ra end-member in the groundwater	190	190	Bq m^{-3}	this study
Q_A	Alongshore transport flux	2.76×10^9		$m^3\ d^{-1}$	Weisberg et al. 2009
$\Delta^{226}Ra^{act}_A$	^{226}Ra activity difference between the two boundary transects (CH and EG)	0.38	0.65	Bq m^{-3}	this study
$TAlk^{inv}$	Excess TAlk inventory in the shelf system	1.13×10^{13}	3.87×10^{12}	mmol	this study
$\Delta TAlk^{con}_A$	TAlk difference between the two boundary transects (CH and EG)	41.5	33.4	mmol m^{-3}	this study
$TAlk^{con}_{RIV}$	TAlk end-member in the estuaries	*see* Table 7		mmol m^{-3}	this study
A'_{SED}	Surface area of benthic sediment	4.6×10^9		m^2	this study
$TAlk^{flux}_{SED}$	Diffusion flux of TAlk from sediments	3.0		mmol $m^{-2}\ d^{-1}$	Krumins et al. 2013
F_{NCP}	Net community productivity in the water column	6.7		mmol $m^{-2}\ d^{-1}$	Hitchcock et al. 2000
DIC^{inv}	Excess DIC inventory in the shelf system	9.93×10^{12}	5.90×10^{12}	mmol	this study
ΔDIC^{con}_A	DIC difference between the two boundary transects (CH and EG)	37.1	68.5	mmol m^{-3}	this study
F_{AIR}	Air–sea exchange of CO_2	6.7×10^{10}	3.3×10^{10}	mmol d^{-1}	this study
DIC^{con}_{RIV}	DIC end-member in the estuaries	*see* Table 7		mmol m^{-3}	this study
DIC^{flux}_{SED}	Diffusion flux of TAlk from sediments	12.9		mmol $m^{-2}\ d^{-1}$	Krumins et al. 2013

* USGS, United States Geological Survey.

where $[ex^{223}Ra : ex\ ^{228}Ra]_{obs}$ denotes the excess Ra ratio in the shelf water, where *ex* means the observed Ra on the shelf minus the background level in the offshore, τ is radium-derived water age, λ_{223} represents the ^{223}Ra decay constant ($\lambda = 1/T_{1/2}$; ^{228}Ra decay can be neglected since its half-life [$T_{1/2} = 5.75$ yr] is long compared with the mixing time scales in our study site), and $[ex^{223}Ra : ex\ ^{228}Ra]_i$ is the Ra AR of the input water. Equation 3 can be rearranged to solve for water age such that:

$$\tau = \left\{ \ln\left[\frac{ex^{223}Ra}{ex^{228}Ra}\right]_i - \ln\left[\frac{ex^{223}Ra}{ex^{228}Ra}\right]_{obs} \right\} / \lambda_{223} \qquad (4)$$

Two assumptions of this water age model are that there is single and uniform radium source, and that no radium removal or addition occurs within the model domain other than mixing and radioactive decay (Moore 2000). Equation 4 is sensitive to variation in the Ra AR of the input water. Since groundwater had very wide $ex^{223}Ra : ex^{228}Ra$ from 0.02 to 7.34, we defined the Ra AR of zero-age water, $[ex^{223}Ra : ex\ ^{228}Ra]_i$, as the ratio found at the station closest to the coast with highest AR. For July and October, the $[ex^{223}Ra : ex^{228}Ra]_i$ was similar at 0.52 and 0.50, respectively. Surface water was well stratified during the two sampling periods except close to the coast (water depth < 10 m); hence, sediment exchange is not a significant source of short-lived Ra to the offshore portion of the model domain.

The calculated water ages ranged from 0 to 76 d and generally increased with distance from shore (Table 1). In July, the average water age was 13 ± 7, 24 ± 7, 31 ± 10, 42 ± 23 d for the 10, 10–20, 20–30, and 30–40 m isotbaths, respectively; in October, it was 15 ± 7, 22 ± 9, 25 ± 5, 59 ± 20 d for the same intervals. The mean water age for the entire study domain with respect to mixing offshore was 28 ± 12 and 30 ± 17 d in July and October, respectively. The error bars are 1 SD of the average, and provide an estimate of the spatial variation in age rather than an uncertainty associated with the method. In terms of cross-shelf mixing, the age method can be translated to a mixing rate from a regression line between water age and offshore distance (figure not shown; Hsieh et al. 2013). For July, this approach yielded a mean cross-shelf rate of 0.028 m s^{-1} ($R^2 = 0.6$), which is the same order of magnitude as an estimate from this region derived from long-term mooring data (0.01 m s^{-1}; Weisberg et al. 2009).

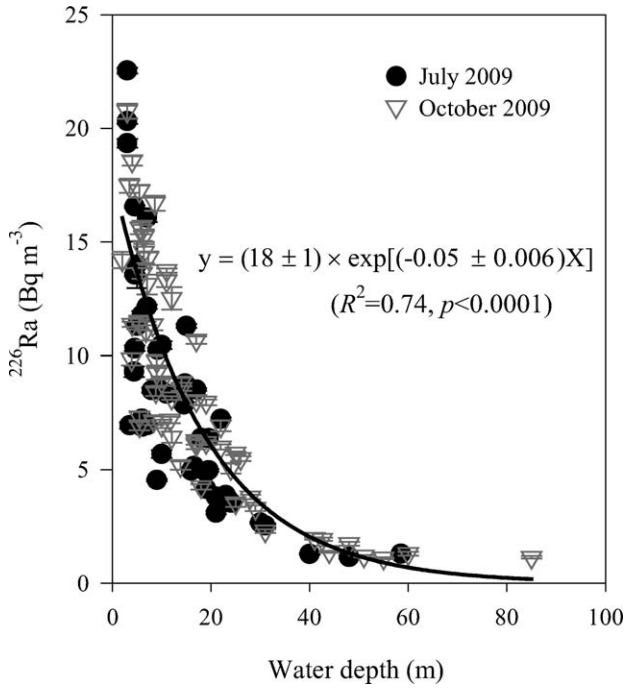

Fig. 9. Radium-226 activity vs. water depth on the southwest Florida Shelf in July and October 2009. Error bars represent counting statistics, which is generally smaller than the symbols. Regression line and equation are displayed.

Ra flux exchange with offshore seawater: We did not collect samples at water depth > 25 m from transects EG1 and EG2 in July, and EG3 to EG4 in October. Hence, we predicted the ^{226}Ra activity in these regions based on the ^{226}Ra relationship with water depth from other transects (Fig. 9). We adopted the approach used in the southeastern U.S. continental shelf (Moore 2007) to calculate the ^{226}Ra inventory. (1) We obtained excess ^{226}Ra in the shelf water by subtracting the background level in the offshore (1.2 Bq m^{-3}). (2) We calculated the product of the average excess ^{226}Ra activity, average water depth, and distance between two adjacent stations to yield the excess ^{226}Ra inventory normalized to shoreline (Bq m^{-1}) in each shore-perpendicular transect. (3) The excess Ra inventory (Bq) was determined by the sum of the ^{226}Ra flux in every shore-perpendicular transect with total shoreline of 210 km. The excess ^{226}Ra inventory can be expressed as the following equation:

$$^{226}\mathrm{Ra}^{\mathrm{inv}} = \sum_{i=1}^{n} 0.5 \times \mathrm{X} \times \sum \mathrm{ex}^{226}\mathrm{Ra} \times z_{\mathrm{ml}} \times \mathrm{y} \qquad (5)$$

where ^{226}Ra$^{\mathrm{inv}}$ is the excess ^{226}Ra inventory; n is the number of shore-perpendicular transects; ex ^{226}Ra, z_{ml}, and y represent average excess ^{226}Ra activity, average mixed-layer depth, and distance in two adjacent stations for each transect, respectively. The distance between two adjacent transects is represented as X.

The excess ^{226}Ra inventory for each transect in July and October are presented in Table 4. We obtained an offshore ^{226}Ra flux of 3.8 ± 1.3 × 10^{10} Bq d^{-1} by using the excess ^{226}Ra inventory divided by water age in July. The ^{226}Ra flux was 5.5 ± 2.5 × 10^{10} Bq d^{-1} and 3.5 ± 2.0 × 10^{10} Bq d^{-1} with and without the TB Transect in October, respectively.

Table 4. The excess ^{226}Ra inventory for each transect along the southwest Florida Shelf in July and October 2009.

Transect	Ex ^{226}Ra inventory (10^6 Bq m^{-1})
July	
CH1	4.3±0.05
CR1	5.3±0.03
CR1a	5.3±0.07
CR1b	2.5±0.03
CR1c	9.2±0.07
EG1	9.0±0.05
EG2	2.8±0.05
October	
TB1	6.5±0.07
CH2	5.2±0.05
CH3	4.7±0.03
CR2	7.8±0.07
CR3	9.7±0.03
CR3a	4.5±0.02
EG3	4.3±0.02
EG4	1.5±0.02

Ra flux from alongshore transport: The alongshore transport for the inner shelf (80 km) is southward with current speeds in the range of 0.01–0.04 m s^{-1} based on long-term mooring data (Weisberg et al. 2009). Using an average rate of 0.02 m s^{-1}, the net transport is 2.76 × 10^9 m^3 d^{-1}. The ^{226}Ra activity in the northern transect boundary (CH) is slightly lower than that in the southern boundary (EG), with a ^{226}Ra activity difference of 0.4 ± 0.1 and 0.6 ± 0.1 Bq m^{-3} in July and October, respectively. Using this Ra imbalance and the net transport rate, we estimate the alongshore transport ^{226}Ra flux to be −0.1 × 10^{10} Bq d^{-1} (July) and −0.2 × 10^{10} Bq d^{-1} (October). The negative values indicate a Ra loss from the model domain and are equivalent to a maximum of 4.9% of the total ^{226}Ra flux.

Riverine Ra flux: River flow rates and riverine ^{226}Ra fluxes are presented in Table 5. If we assume all of the particulate ^{226}Ra from freshwater discharge desorbs upon entering the CRE, this process would produce 0.1 × 10^7 and 0.07 × 10^6 Bq d^{-1} in July and October, which is < 6% of the riverine dissolved ^{226}Ra. Even though particulate ^{226}Ra is likely unimportant, to avoid underestimating riverine ^{226}Ra contribution we used the intercept of the ^{226}Ra linear relationship with salinity to obtain the effective ^{226}Ra activity in the end-member of individual rivers along the SWFS. This effective activity represents the sum of the ^{226}Ra contributions from the estuary (particulate plus dissolved; Table 5); it would also account for direct SGD input to the estuaries. Hence, our SGD estimates are for direct input to the SWFS only. We calculated the individual riverine ^{226}Ra flux by multiplying the river flow rate with the corresponding effective ^{226}Ra activity. It should be

Table 5. Monthly river flow rates and riverine ^{226}Ra fluxes along the southwest Florida Shelf in July and October 2009.

Estuary	River flow rate (m^3 s^{-1}) Jul	Oct	Effective ^{226}Ra end-member (Bq m^{-3})	Riverine ^{226}Ra flux ($\times 10^8$ Bq d^{-1}) Jul	Oct	River gauge No.	River name
Charlotte Harbor	38	9	40	1.6	0.4	USGS 2296750	Peace River
	8	4				USGS 02298830	Myakka River
Caloosahatchee estuary	101	6	38	3.3	0.2	USGS 02292900	Caloosahatchee River
Shark River estuary	19	12	94	1.6	1	USGS 252230081021300	Shark River
Tampa Bay	—	1	78	—	0.5	USGS 02304500	Hillsborough River
	—	5				USGS 02301500	Alafia River
	—	2				USGS 02300500	Little Manatee River

All of the river flow rates were downloaded from United States Geological Survey (USGS) Web page "USGS Surface-Water Data for the Nation" (http://waterdata.usgs.gov/nwis/sw).

noted that we assumed the effective ^{226}Ra was constant for each estuary in July and October because we only collected samples from the SRE in July and from the other three estuaries in October. We also note that these effective riverine ^{226}Ra end-members were based upon limited data, ranging from 3–7 sampling stations per estuary. Despite these uncertainties, the total flux from the four estuaries provided only 1.6% (0.06×10^{10} Bq d^{-1}) and 0.4% (0.02×10^{10} Bq d^{-1}) of the total ^{226}Ra flux to the SWFS in July and October, respectively.

Ra flux from sediment diffusion: Another potential ^{226}Ra source could be sediment release, i.e., the diffusion from the sediment of regenerated ^{226}Ra produced by radioactive decay of particle-bound ^{230}Th. For similar studies from this region, sediment contributed 0.002 Bq m^2 d^{-1} in Tampa Bay (Swarzenski et al. 2007) and 0.02 Bq m^2 d^{-1} in Charlotte Harbor (Miller et al. 1990). Here, we adopted the relatively high value of 0.02 Bq m^2 d^{-1} as the sediment diffusion rate in our box model, which was greater than global average of 0.007 Bq m^2 d^{-1} (Beck et al. 2007). To avoid underestimation of the potential sediment contribution, we applied the benthic flux to the whole study area (1.38×10^{10} m^2) and derived a sediment release of 0.03×10^{10} Bq d^{-1}, which represents only 0.9% of the total ^{226}Ra flux.

Ra flux from hydrothermal springs: Eight hydrothermal submarine springs have been identified along the coast at water depths of 12–14 m, and all were enriched in ^{226}Ra (1717 Bq m^{-3}; Fanning et al. 1981) 1000-fold compared to the seawater. Thus, hydrothermal springs could be a ^{226}Ra source to the inner shelf. To our knowledge, the discharge rate was only estimated for a single vent (Mud Hole submarine spring [MHSS]), which was reported to be 25 L s^{-1} (Fanning et al. 1981). If we assume that the other seven hydrothermal springs have similar ^{226}Ra and discharge rates as MHSS, we estimate the total hydrothermal ^{226}Ra to the SWFS to be 3×10^7 Bq d^{-1}, $< 0.1\%$ of the total ^{226}Ra flux. This is qualitatively supported by the relatively low ^{226}Ra enrichments in bottom water near the MHSS noted earlier.

SGD fluxes: Based on Eq. 2, we estimate that the ^{226}Ra flux contributed by SGD was equivalent to 98–99% of the total ^{226}Ra flux (Table 6). Using SGD-derived ^{226}Ra fluxes and average ^{226}Ra in groundwater (183 Bq m^{-3}, excluding hydrothermal springs), the total SGD flux was $20 \pm 10 \times 10^7$ m^3 d^{-1} in July, and $18 \pm 8 \times 10^7$ and $28 \pm 14 \times 10^7$ m^3 d^{-1} without and with the TB Transect in October. If we take a more conservative approach and assume that the groundwater end-member ^{226}Ra activity is equal to our maximum observed value of 3750 Bq m^{-3}, we can obtain a minimum SGD flux of $1.0 \pm 0.9 \times 10^7$ m^3 d^{-1} in July, $0.9 \pm 0.6 \times 10^7$ and $1.4 \pm 0.7 \times 10^7$ m^3 d^{-1} without and with the TB Transect in October. It should be noted that our estimated SGD flux was for direct input to the SWFS and excluded groundwater discharged within the major

Table 6. All ^{226}Ra input and output fluxes and their fraction of the total Ra flux on the southwest Florida Shelf in July and October 2009.

	July		October	
	^{226}Ra flux ($\times 10^8$ Bq d^{-1})	Percentage of total ^{226}Ra flux (%)	^{226}Ra flux ($\times 10^8$ Bq d^{-1})	Percentage of total ^{226}Ra flux (%)
Input				
Local rivers	6.5	1.6	1.6	0.4
Sediment diffusion	3.2	0.8	3.2	0.9
Hydrothermal spring	0.2	0.06	0.2	0.06
SGD	386	98	357	99
Output				
Mixing with offshore	385	97	344	95
Net alongshore transport	10.7	2.7	17.7	4.9

estuaries and via submarine thermal springs. For the 210 km coastline length of our model domain, these SGD fluxes correspond to shoreline-normalized rates of 882–955 $m^3\ m^{-1}\ d^{-1}$. Our values are on par with or slightly lower than other regional-scale studies, such as the northeast Gulf of Mexico (620–2450 $m^3\ m^{-1}\ d^{-1}$, assumed shoreline length of 25 km; Cable et al. 1996), South Atlantic Bight (918–1032 $m^3\ m^{-1}\ d^{-1}$; Moore 2010), and the northern South China Sea (1104–1201 $m^3\ m^{-1}\ d^{-1}$; Liu et al. 2012).

SGD flux uncertainty analysis: The cumulative ^{226}Ra inputs to the SWFS from rivers, sediment diffusion, and hydrothermal springs were small, in total representing only a few percent of the total ^{226}Ra budget (Table 6). Thus, at steady state, the input of ^{226}Ra via SGD (the only important source of ^{226}Ra) will be balanced by the major sink for ^{226}Ra over the shelf: mixing with offshore seawater. In our model, this offshore mixing term is calculated from the excess ^{226}Ra inventory and the average water age within the study domain, estimated using ^{223}Ra and ^{228}Ra (Eq. 4). The uncertainty in the excess ^{226}Ra inventory is mainly from the measurement error for ^{226}Ra, which was only 0.3% of the total inventory. However, a variation of 1 d in the average water age would lead to a 5–6% change in the SGD flux. The average water age in our study area has a standard deviation of 12 d and 17 d in July and October, respectively, though much of this variability is natural, as water age is expected to vary with distance from the coastline (Moore 2000). A more appropriate approach for calculating uncertainty on the water age is to propagate the error associated with the $^{223}Ra : {}^{228}Ra$ initial value assumption. The initial ratio variation was only 4% based on our observation in July and October, which would change the water age by up to 1.1 d, suggesting this had minor effect on SGD–^{226}Ra flux in our continental shelf. In addition, alongshore transport, which is calculated from the north–south boundary ^{226}Ra activity difference and alongshore transport rate, is a potential uncertainty source. The uncertainty of the boundary ^{226}Ra difference derived from measurement error propagation in July and October was 0.1 Bq m^{-3}, which would change the estimated SGD flux by $< 1\%$. Since we used the alongshore velocity (0.02 m s^{-1}) from long-term mooring data, variability at the time of our cruises is not accounted for. However, a 100% variation of alongshore transport rate would result in a relatively minor 1–5% change in the SGD flux. As noted earlier, groundwater displayed a wide range of ^{226}Ra activities and a 10% change in the groundwater average would drive a similar change in our calculated SGD flux. Thus, the biggest uncertainty in our SGD estimate is derived from the uncertainty in the groundwater ^{226}Ra end-member. However, the observed variability is due to the heterogeneous nature of various aquifer properties that control groundwater Ra isotope activities. For these reasons, placing an exact value on the uncertainty in our SGD flux estimate due ^{226}Ra end-member variation is a difficult task.

Groundwater recharge balance: The recharge rate of the freshwater aquifers along the shoreline of SWFS depends on rainfall, watershed area, and evapotranspiration. It can be represented mathematically as follows (Kelly and Moran 2002):

$$Q_r = (1-\varphi) \times \sum A \times P \quad (6)$$

where Q_r represents the aquifer recharge rate; φ is the evapotranspiration factor taking into account the loss of precipitation by both runoff and evapotranspiration (here we used 0.7 for southern Florida; Jiang et al. 2009). In our case, A is the watershed area (m^2) and P corresponds to annual rainfall (mm) from 01 August 2008 to 01 August 2009. The total watershed consists of the Peace River ($3.5 \times 10^9\ m^2$; 96 mm), Myakka River ($1.6 \times 10^9\ m^2$; 82 mm), Caloosahatchee River ($4.4 \times 10^9\ m^2$; 129 mm), and Everglades ($1.0 \times 10^{10}\ m^2$; 136 mm) watersheds. By solving Eq. 6, the aquifer recharge rate was estimated to be $2.0 \times 10^7\ m^3\ d^{-1}$ for the year 2008–2009. Terrestrial groundwater discharge must be in balance with aquifer recharge if we do not take into account groundwater withdrawal for agriculture and municipal uses. Excluding potential deep terrestrial groundwater sources, this flux is comparable to or greater than total local river flow ($1.4 \times 10^7\ m^3\ d^{-1}$ in July; $0.3 \times 10^7\ m^3\ d^{-1}$ in October; Table 5) and equivalent to $\sim 10\%$ of the average SGD flux and, hence, our radium-derived SGD fluxes must include primarily marine groundwater. In theory, we can use the average salinity of the SGD to estimate the terrestrial SGD flux and compare it with the result derived from groundwater recharge balance. However, we only had groundwater salinity data along the CRE rather than from all the regions near the SWFS coast. Thus, this approach does not apply to our study due to the lack of salinity data over a wider geographical region.

TAlk and DIC fluxes from SGD—To compare SGD-related chemical constituents between July and October, we focus only on data from stations common to both the July and October cruises, i.e., we exclude the results that include the October TB Transect for the remainder of the discussion.

SGD-derived TAlk and DIC fluxes using the ^{226}Ra box model: Generally speaking, TAlk and DIC fluxes due to terrestrial groundwater are estimated by multiplying the terrestrial groundwater TAlk and DIC end-members (5371 and 6175 $\mu mol\ L^{-1}$) with the terrestrial component of the SGD flux. A similar approach is taken for the marine groundwater end-members with one key exception: we must account for the fact that marine groundwater is sourced from coastal seawater, which will include significant preformed TAlk and DIC during recharge. We therefore use the marine SGD flux combined with average difference between seawater and marine groundwater for TAlk (2083 $\mu mol\ L^{-1}$ in July; 2115 $\mu mol\ L^{-1}$ in October) and DIC (3088 $\mu mol\ L^{-1}$ in July; 3119 $\mu mol\ L^{-1}$ in October). Therefore, TAlk and DIC end-members in terrestrial groundwater are greater than the difference between marine groundwater and seawater for TAlk and DIC. Since marine SGD is the dominant component of total SGD ($\geq 90\%$), to avoid overestimation, we only use our ^{226}Ra-derived SGD estimates and the TAlk and DIC difference between marine groundwater and seawater to

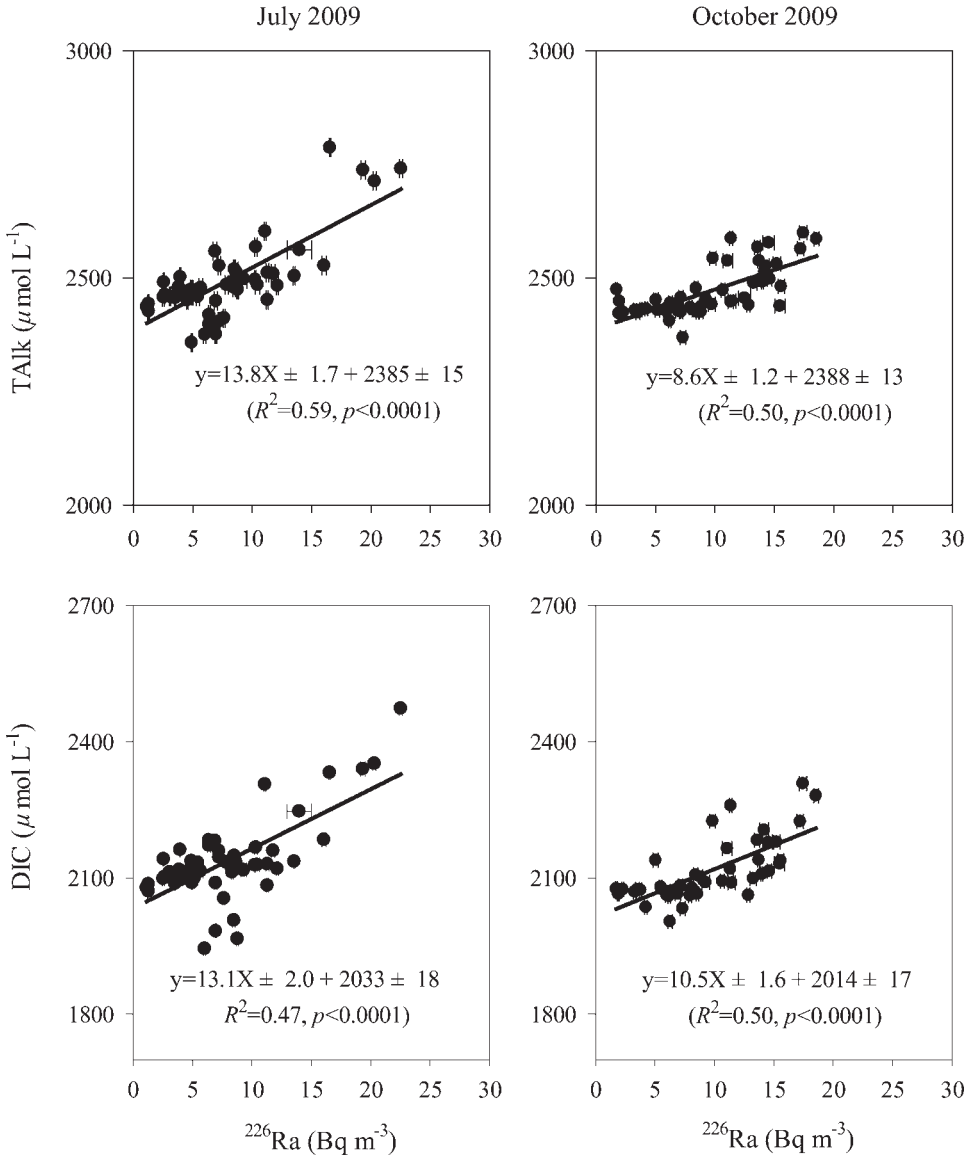

Fig. 10. Total alkalinity (TAlk) and dissolved inorganic carbon (DIC) vs. ^{226}Ra in the shelf water on the southwest Florida Shelf in July and October 2009. Regression line and equations are also shown.

derive an SGD–TAlk flux of $4.2 \pm 2.0 \times 10^8$ and $3.9 \pm 1.5 \times 10^8$ mol d^{-1}, and SGD–DIC flux of $6.2 \pm 2.3 \times 10^8$ and $5.8 \pm 1.9 \times 10^8$ mol d^{-1} in July and October, respectively.

In addition to SGD, we must consider TAlk and DIC contributions from benthic diffusion in the shallow region due to organic matter degradation by various autotrophic and heterotrophic benthic communities (Phillips et al. 1990) as well as sediment carbonate dissolution. To the south of Charlotte Harbor, carbonate sands dominate (mean 75%) with organic content ranging from 2.3% to 2.5% (Hammerstrom et al. 2006). Unfortunately, no data are known for the benthic inorganic carbon cycle in our continental shelf region. However, if we adopted the global average benthic TAlk and DIC flux for marine carbonate shelves of 3 and 12.9 mmol m^{-2} d^{-1}, respectively (Krumins et al. 2013), these fluxes would equal 1.4×10^7 mol d^{-1} TAlk and 5.9×10^7 mol d^{-1} DIC within our study domain. These benthic diffusion fluxes are one order of magnitude lower than the groundwater contribution.

TAlk and DIC fluxes estimated from the shelf-water TAlk– and DIC–^{226}Ra relationships: A significant ($p < 0.001$) positive correlation existed between TAlk and DIC concentrations and ^{226}Ra over the shelf (Fig. 10). One end-member is the offshore seawater (Gulf of Mexico), which was characterized by low TAlk, DIC, and ^{226}Ra; the other end-member was elevated in all three properties, which we assume must be derived from groundwater. Therefore, we can estimate the SGD-derived TAlk and DIC fluxes from the product of TAlk : ^{226}Ra (13.8 mmol Bq^{-1} in July; 8.6 mmol Bq^{-1} in October) and DIC : ^{226}Ra ratio (13.1 mmol Bq^{-1} in July; 10.5 mmol Bq^{-1} in October) and the SGD-derived ^{226}Ra flux. This suggests a total groundwater TAlk

Table 7. Total alkalinity (TAlk) and dissolved inorganic carbon (DIC) concentrations in the fresh, saline groundwater (GW), Charlotte Harbor, Caloosahatchee River, and Shark River. TAlk and DIC fluxes discharged by submarine groundwater discharge (SGD), and rivers to the southwest Florida Shelf (SWFS) in July and October 2009.

	TAlk range (μmol L^{-1})	TAlk (μmol L^{-1})	DIC range (μmol L^{-1})	DIC (μmol L^{-1})	Mean TAlk flux ($\times 10^6$ mol d^{-1})		Mean TAlk flux ($\times 10^6$ mol d^{-1})		Mean DIC flux ($\times 10^6$ mol d^{-1})		Mean DIC flux ($\times 10^6$ mol d^{-1})	
					July		October		July		October	
Fresh GW	2375–6914	5371*	3885–8082	6175*	—		—		—		—	
Saline GW	3201–8030	4578*	3332–8422	5227*	—		—		—		—	
Total SGD†	—	—	—	—	418±390		392±240		619±280		578±190	
Total SGD‡	—	—	—	—	465±390		297±160		490±280		390±190	
Total SGD§	—	—	—	—	453±176		186±31		518±245		443±156	
Charlotte Harbor	1446–2448	1502‖	1525–2120	1568‖	6		2		6		2	
Caloosahatchee River	1120–3341	2787‖	779–3491	2798‖	24		1		24		1	
Shark River	2534–3418	3778‖	2306–4016	4805‖	6		4		8		5	
Total rivers	—	—	—	—	36		7		38		8	
Total SGD : total rivers	—	—	—	—	11–13		26–56		13–16		48–71	

* Mean TAlk and DIC concentrations.
† SGD–TAlk, SGD–DIC fluxes were derived from the product of SGD flux and TAlk, DIC concentrations difference between groundwater and average seawater.
‡ SGD–TAlk, SGD–DIC fluxes were derived from the product of ^{226}Ra flux from SGD and TAlk : ^{226}Ra; ^{226}Ra flux from SGD and DIC : ^{226}Ra in the shelf water.
§ SGD–TAlk, SGD–DIC fluxes were obtained by TAlk and DIC budgets in the shelf water.
‖ Effective TAlk and DIC concentrations.

flux to the SWFS of 4.6 ± 3.9 × 10^8 and 3.0 ± 1.6 × 10^8 mol d^{-1} in July and October, respectively. The DIC flux associated with SGD was 4.9 ± 2.8 × 10^8 mol d^{-1} (July) and 3.9 ± 1.9 × 10^8 mol d^{-1} (October). It should be noted that ^{226}Ra should display relatively conservative behavior in the shelf water once it is discharged from groundwater, while TAlk and DIC may be influenced by biological activity and other nonconservative addition or removal processes. However, the linear relationship between ^{226}Ra and TAlk and DIC would indicate that these processes were minimal, though other controlling processes cannot be ruled out since the correlation coefficient ($R^2 \approx 0.5$) was somewhat low.

TAlk and DIC fluxes from rivers—For comparison, the TAlk and DIC fluxes from local rivers were determined by multiplying individual river fluxes (Table 5) by the effective TAlk and DIC concentrations in the river extrapolated from the linear regression (Table 7). The average TAlk input by total SGD was 11–56-fold greater than the sum of local rivers, while the average DIC flux contributed by total SGD exceeded the river flux by a factor of 13–71. Our estimated average SGD-delivered TAlk and DIC fluxes to the SWFS were 10–15%, and 13–20% of those from the Mississippi River (Cai 2003). Given that our study focused on only an ~ 200 km stretch of coastline, it is likely that SGD plays dominant role in supplying TAlk and DIC to the Gulf of Mexico.

TAlk and DIC mass balance—In order to assess the significance of SGD's contribution to the TAlk and DIC budget over the SWFS, we constructed steady-state TAlk and DIC mass balances with consideration for all potential sources and sinks. The internal fluxes included calcium carbonate production or dissolution and net community production (NCP) in the water column and shallow seafloor. The TAlk and DIC mass balances can be expressed as follows:

$$\begin{aligned} &\frac{\mathrm{TAlk}^{\mathrm{inv}}}{\tau} \pm (\mathrm{Q_A} \times \Delta\mathrm{TAlk_A^{con}}) \pm \mathrm{F_{CA}} \\ &\quad = \left(\sum [\mathrm{Q_{RIV}} \times \mathrm{TAlk_{RIV}^{con}}]\right) + \left(\mathrm{A'_{SED}} \times \mathrm{TAlk_{SED}^{flux}}\right) \\ &\quad + \left(\frac{17}{106}\mathrm{F_{NCP}}\right) + \mathrm{FTAlk_{SGD}} \end{aligned} \tag{7}$$

$$\begin{aligned} &\frac{\mathrm{DIC}^{\mathrm{inv}}}{\tau} \pm \left(\mathrm{Q_A} \times \Delta\mathrm{DIC_A^{con}}\right) \pm \left(\frac{1}{2}\mathrm{F_{CA}}\right) \\ &\quad + \mathrm{F_{NCP}} \pm \mathrm{F_{AIR}} = \left(\sum [\mathrm{Q_{RIV}} \times \mathrm{DIC_{RIV}^{con}}]\right) \\ &\quad + \left(\mathrm{A'_{SED}} \times \mathrm{DIC_{SED}^{flux}}\right) + \mathrm{FDIC_{SGD}} \end{aligned} \tag{8}$$

where the left-hand side of the equations includes the total TAlk and DIC outputs, and the right-hand side includes the inputs. $\mathrm{TAlk}^{\mathrm{inv}}/\tau$ and $\mathrm{DIC}^{\mathrm{inv}}/\tau$ denote TAlk and DIC mixing with offshore seawater (mol d^{-1}). $\mathrm{TAlk}^{\mathrm{inv}}$ and $\mathrm{DIC}^{\mathrm{inv}}$ are excess inventories of TAlk and DIC (mol) subtracting the background values for offshore seawater.

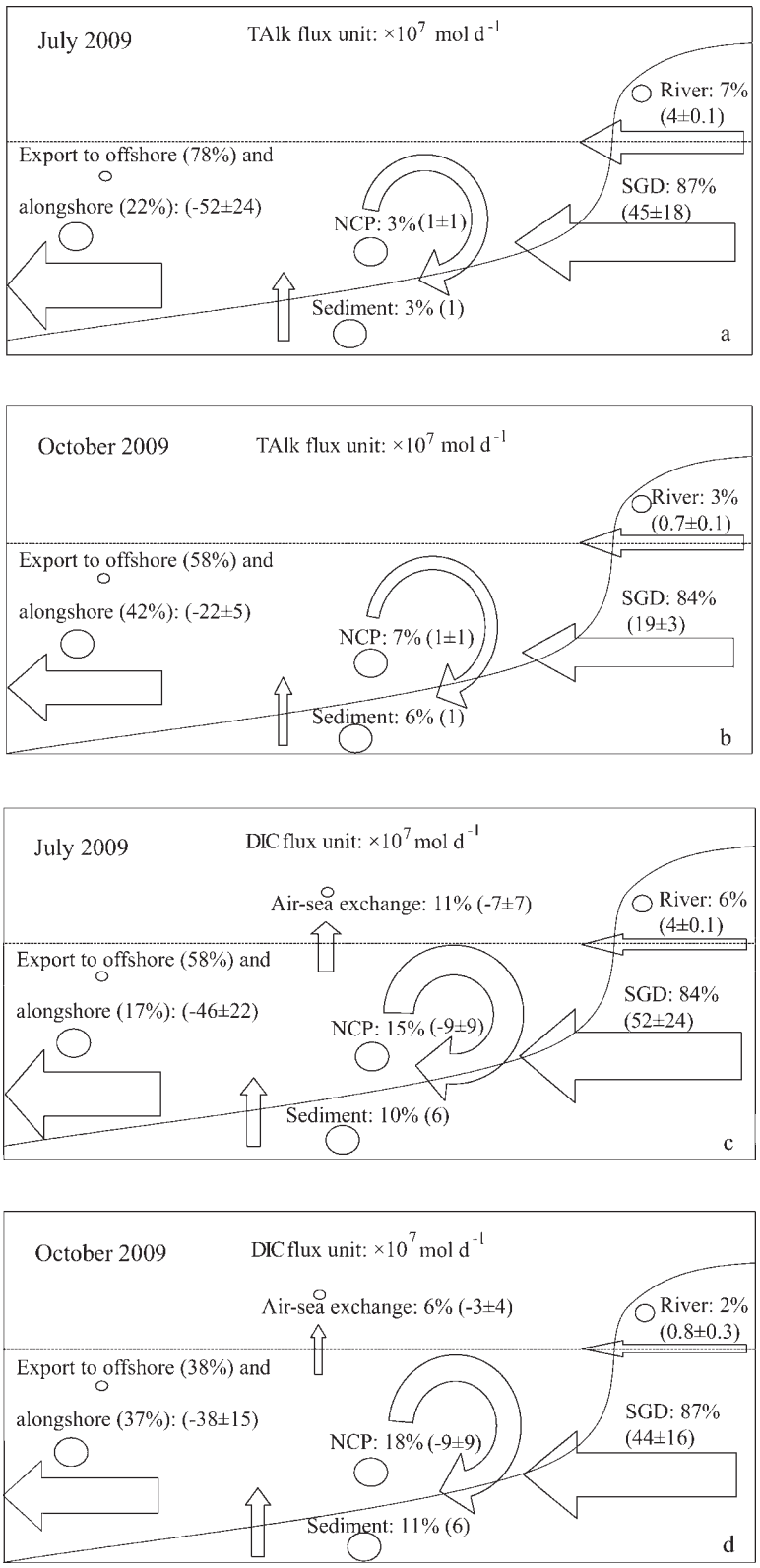

Fig. 11. Sources and sinks of total alkalinity (TAlk) and dissolved inorganic carbon (DIC) on the southwest Florida Shelf in (a, c) July and (b, d) October 2009 derived from a TAlk and DIC mass balance. River input, submarine groundwater discharge (SGD), sediment input, and net community production (NCP) in the water column are net TAlk sources in both July and October. Export to offshore and alongshore transport are the main TAlk sinks in both July and October. River input, SGD, and sediment diffusion are net DIC sources. Export to

Here, we used a similar approach to the ^{226}Ra inventory estimate; however, unlike ^{226}Ra, no significant relationship existed between TAlk, DIC, and water depth in the shelf water. We therefore interpolated the TAlk and DIC concentrations by a linear Kriging interpolation method to grid data points (SURFERTM by Golden Software) for the 25 m to 40 m isobaths in the southern portion (EG1, EG2, EG3, and EG4) of the SWFS where we lacked adequate sampling resolution.

There are clear differences in TAlk and DIC between the northern- (CH) and southern-most (EG) transects (41 μmol L^{-1} and 32 μmol L^{-1} for $\Delta TAlk_A^{con}$ in July and October; 37 μmol L^{-1} and 68 μmol L^{-1} for ΔDIC_A^{con} in July and October); therefore, we must include an alongshore flux component in our model. For this, we need the average alongshore transport rate (Q_A), which is 0.02 m s^{-1} based on long-term mooring data (Weisberg et al. 2009). F_{CA} represents the calcium carbonate precipitation (sink) or dissolution (source). The calcite or aragonite saturation index (Ω) was calculated from $\Omega = [Ca^{2+}][CO_3^{2-}]/Ksp$, where Ksp is the $CaCO_3$ solubility product (Mucci 1983). Ca^{2+} in the shelf water was derived from the observed salinity (S) at the seawater during the cruises assuming a constant Ca : S ratio (Ca^{2+} [μmol kg^{-1}] = 10,280 × S/35; Millero 2005). CO_3^{2-} concentration was calculated from DIC and TAlk with the program CO2SYS (Lewis and Wallace 1998). The dissociation constants of carbonic acid were taken from Millero et al. (2006). The CO_2 solubility coefficient was taken from Weiss (1974) and the sulfate dissociation constant from Dickson (1990). The main carbonate production is coralline algal growth with water depths of 60–80 m (Phillips et al. 1990); our study area is largely devoid of these coral reef settings (Hine et al. 2008); also, $CaCO_3$ formation is not observed in the northern of Gulf of Mexico during mixing with Mississippi River plume, where the calcite saturation index was as high as 5–12 (Guo et al. 2012). The saturation index was 4–7 for calcite and 3–4 for aragonite in our study area, which is close to the average saturation state (5–6 for calcite and 3–4 for aragonite) in subtropical surface seawater, which largely rules out the possibility of carbonate dissolution. Because there are no estimates of $CaCO_3$ precipitation or dissolution rate for the SWFS, here, we do not include this term in our estimates.

F_{NCP} is net community productivity. The primary production rate in the water column of the West Florida Shelf during non-bloom conditions ranges from 5–42 mmol m^{-2} d^{-1} (Vargo et al. 1987). Using the oxygen isotope method over the West Florida Shelf after the spring bloom, Hitchcock et al. (2000) reported that respiration rates nearly balanced phytoplankton production with a mean NCP rate of 6 ± 6 mmol m^{-2} d^{-1}. Since we did not observe any algal blooms during our cruises, we adopted 6 mmol m^{-2} d^{-1} as the water column NCP rate.

Benthic organisms may play an important role in the primary production of the clear, oligotrophic ocean off West Florida Shelf (Phillips et al. 1990). Based on sediment incubation experiments in the northeast Gulf of Mexico (Chipman 2011) and South Atlantic Bight, gross benthic primary production (BPP) is roughly equal to benthic respiration. For example, though the gross BPP in the South Atlantic Bight was equivalent to 56% of the water column productivity, the net BPP was only 1.4 mmol m^{-2} d^{-1} (Jahnke et al. 2000). Since there is no net BPP estimate in our study domain and considering that it is very likely to have a minor effect on the inorganic carbon budget, we neglected this item in our TAlk and DIC box models.

The calculation of the air–sea exchange flux (F_{AIR}) was calculated using $F_{AIR} = k \times K_H \times (P_{CO_2}^{sea} - P_{CO_2}^{air})$, where k is the gas transfer velocity of CO_2 (cm h^{-1}); K_H is the CO_2 solubility in seawater (Weiss 1974); $(P_{CO_2}^{sea} - P_{CO_2}^{air})$ is the mean sea–air P_{CO_2} difference. The partial pressure of CO_2 was calculated from measured TAlk and DIC using CO_2SYS.XLS 14th version (http://www.ecy.wa.gov/programs/eap/models.html) using the same constants as with the CO_3^{2-}. The atmospheric P_{CO_2} ($P_{CO_2}^{air}$) was set as constant based on the mean atmospheric CO_2 concentration during an August 2009 cruise over the West Florida Shelf (39.5 ± 1.2 Pa, i.e., 390 ± 12 μatm; Robbins et al. 2010*a*). We use the equation in Wanninkhof (1992) to obtain k, $k = f \times (u_{10})^2 \times (Sc/660)^{-0.5}$, where f denotes the proportionality factor, 0.39 for long-term winds; u_{10} represents wind speed at 10 m, which averaged 4.0 and 3.9 m s^{-1} in July and October 2009, respectively (National Oceanic and Atmospheric Administration Sta. NFBF1, wind speed data are from the Web page "National Data Buoy Center," http://www.ndbc.noaa.gov/); Sc is the Schmidt number of CO_2 in seawater. We neglected CO_2 production from photochemistry in our DIC budget because this effect is insignificant in the wet season based on a diurnal and seasonal study of the SWFS by Clark et al. (2004). The SWFS released 5 and 2 mmol m^{-2} d^{-1} (-7×10^7 and -3×10^7 mol d^{-1}; Fig. 11) CO_2 to the atmosphere in July and October, which is consistent with previous studies that suggest the West Florida Shelf is a stronger CO_2 source to the atmosphere in July (7.5 mmol m^{-2} d^{-1}) than in October (0.8 mmol m^{-2} d^{-1}; Walsh et al. 2003). Robbins et al. (2010*a*,*b*) measured underway P_{CO_2} data over the West Florida Shelf in 2009, and concluded that the West Florida Shelf was a net CO_2 source to the atmosphere.

A number of factors affect shelf-water P_{CO_2}, including temperature, water mass mixing, terrestrial inputs (SGD and river), upwelling, primary production, respiration, remineralization, and biogenic calcification or dissolution. Temperature-normalized P_{CO_2} in July was still greater than

---

←

offshore, alongshore transport, and air–sea CO_2 exchange are DIC sinks. Circle size from big to small denotes the level of uncertainty in fluxes from high to low. Percentage values represent the fraction of the respective TAlk and DIC input and output fluxes. The number in parentheses after the percentage is the TAlk or DIC flux in units of $\times 10^7$ mol d^{-1}, where positive values represent a source and negative values indicate a sink.

in October. Due to the uncertainty in the $CaCO_3$ dissolution or precipitation and NCP terms, we cannot draw firm conclusions as to why the air–sea CO_2 exchange flux was different in July and October. However, given the major DIC contribution from groundwater, SGD may be one of the more important factors driving P_{CO_2} for this shelf system. The SWFS generally releases CO_2 to the atmosphere in the summer and absorbs atmospheric CO_2 in the winter (Coble at al. 2010). This may be driven by the high rates of SGD-derived DIC fluxes during the summertime wet season as observed in this study, though the exact relationship between precipitation, SGD, and P_{CO_2} over continental shelves needs to be explored in a future study.

$\sum [Q_{RIV} \times TAlk_{RIV}^{con}]$ and $\sum [Q_{RIV} \times DIC_{RIV}^{con}]$ are the sum of TAlk and DIC fluxes of local rivers, which are listed in Table 7. A'_{SED} is the bottom area of inner shelf (4.6×10^9 m^2); $TAlk_{SED}^{flux}$ and DIC_{SED}^{flux} represent TAlk and DIC benthic diffusion (mmol m^{-2} d^{-1}), which has been discussed earlier. $FTAlk_{SGD}$ and $FDIC_{SGD}$ denote average TAlk and DIC fluxes via total SGD. All the terms are known, except $FTAlk_{SGD}$ and $FDIC_{SGD}$. Therefore, we can estimate these two rates by solving Eqs. 7 and 8 (Table 3).

The significance of SGD in the TAlk and DIC budgets: The resulting TAlk and DIC sources and sinks are presented in Fig. 11. We obtained SGD-derived TAlk fluxes of $4.5 \pm 1.8 \times 10^8$ and $1.9 \pm 0.3 \times 10^8$ mol d^{-1}, DIC fluxes of $5.2 \pm 2.4 \times 10^8$ and $4.4 \pm 1.6 \times 10^8$ mol d^{-1} in July and October 2009, respectively. SGD delivered 87% and 84% of the total TAlk input to the SWFS in July and October, and SGD-associated DIC fluxes represented 84% and 87% of the total DIC inputs to the SWFS in July and October. These fluxes were basically consistent with those derived from the ^{226}Ra box model.

The best constrained fluxes in our model are the air–sea flux of CO_2 and shelf–Gulf of Mexico exchange terms. The sediment diffusion and river fluxes are less well known, due to limited sample size, but these sources contribute only ~ 2–11% of the TAlk and DIC inputs to the SWFS. The fluxes with the largest uncertainty include NCP, alongshore transport, and calcium carbonate precipitation or dissolution. To assess the effect of these uncertainties, we performed a simple sensitivity analysis with these terms. A 100% variation in NCP and alongshore transport would change the SGD–TAlk flux by 2–55% and the SGD–DIC flux by 9–45%. Any unrecognized calcium carbonate precipitation would lead to even stronger SGD sources for TAlk and DIC because more TAlk and DIC from SGD would be needed to balance these sinks based on Eqs. 7 and 8. In either case, SGD would remain the major DIC and TAlk source over the SWFS. However, to better constrain future TAlk and DIC budgets for the SWFS, biological sources and sinks as well as physical transport terms must be explicitly measured. Despite these uncertainties in the TAlk, DIC, and ^{226}Ra mass balances, comparable SGD-derived TAlk and DIC fluxes using these two independent approaches gives us confidence in the accuracy of our estimates.

In summary, the SGD into the SWFS was estimated to be $20 \pm 10 \times 10^7$ and $18 \pm 8 \times 10^7$ m^3 d^{-1} in July and October 2009. Approximately 2×10^7 m^3 d^{-1} (~ 10%) was terrestrial groundwater, suggesting that the freshwater SGD fluxes were the same order of magnitude as the river discharge of 1.4×10^7 m^3 d^{-1} in July 2009. It should be noted that our SGD estimates are for direct input to the SWFS only, excluding groundwater discharged to the Gulf of Mexico from the major estuaries. For example, the average SGD rate into the CRE alone was $4.5 \pm 5.5 \times 10^5$ m^3 d^{-1} from 2009 to 2010, or 45% of the Caloosahatchee River flux (Charette et al. 2013). Hence, if we consider the estuarine SGD contribution, the SGD flux to the SWFS will be higher than current estimate. During the 2009 wet season, SGD delivered 28–45 mmol m^{-2} d^{-1} DIC and 13–34 mmol m^{-2} d^{-1} TAlk to the SWFS. These values are comparable to a river-dominated continental shelf in the northern South China Sea (SGD–DIC flux: 16–36 mmol m^{-2} d^{-1}; Liu et al. 2012), and a coral reef lagoon in the South Pacific (SGD–TAlk flux: 60–67 mmol m^{-2} d^{-1}; Cyronak et al. 2013), but lower than those from other local-scale systems, such as a South Carolina salt marsh (SGD–DIC flux: 171 mmol m^{-2} d^{-1}; Cai et al. 2003) and an Australian mangrove estuary (SGD–DIC flux: 250 mmol m^{-2} d^{-1}; Maher et al. 2013).

To our knowledge, this study provides the first comprehensive evaluation of the shelf-scale SGD contribution to the carbon cycle in a carbonate coastal system. Although the importance of groundwater as a carbon source to the coastal ocean has been previously noted (Najjar et al. 2010), it has not been included in coastal carbon budgets (Coble at al. 2010, in the Gulf of Mexico). If SGD from carbonate aquifers accounts for 12% of global terrestrial groundwater discharge (~ 290 km^3 yr^{-1}; Beck et al. 2013) and the DIC end-member in karst groundwater is similar to our study (~ 6200 μmol L^{-1}), then karst SGD systems could supply 1.8 Tmol DIC to the coastal ocean annually (equivalent to 5% of global riverine DIC flux; Cai 2011). If marine SGD is roughly a factor of 10 higher than terrestrial SGD in these systems (Moore et al. 2010), then multiplying this flux with the average DIC concentration difference between marine groundwater and seawater (~ 3100 μmol L^{-1}) produces a marine SGD–DIC flux of ~ 8.0 Tmol yr^{-1} DIC to the ocean, or 24% of the global riverine DIC flux. Future studies of carbon cycling on carbonate-dominated continental shelves should consider the role of SGD on the carbon budget of the coastal ocean.

Acknowledgments

We thank Larry Brand for organizing these cruises and providing conductivity–temperature–depth data, and Adina Paytan for providing long-lived Ra data in the groundwater of Everglades. We thank Michael Holcomb and Rebecca Belastock for help with the dissolved inorganic carbon and total alkalinity measurements. Crystal Breier, Yoonja Kang, and the crew of the R/V *F. G. Walton Smith* assisted with field sampling in the shelf water and groundwater. We are also grateful to the inspiring comments from Willard Moore and Shuh-Ji Kao. Constructive comments by Michiel Rutgers van der Loeff and an anonymous reviewer on the original manuscripts are highly appreciated. This work was supported by funding from the National Science Foundation Chemical Oceanography Program (grant OCE-0751525 to M.A.C.) and the Cove Point Foundation (M.A.C.).

References

Beck, A. J., M. A. Charette, J. Kirk Cochran, M. E. Gonneea, and B. Peucker-Ehrenbrink. 2013. Dissolved strontium in the subterranean estuary—implications for the marine strontium isotope budget. Geochim. Cosmochim. Acta **117:** 33–52, doi:10.1016/j.gca.2013.03.021

———, J. P. Rapaglia, J. K. Cochran, and H. J. Bokuniewicz. 2007. Radium mass-balance in Jamaica Bay, NY: Evidence for a substantial flux of submarine groundwater. Mar. Chem. **106:** 419–441, doi:10.1016/j.marchem.2007.03.008

Boyle, E. A., D. F. Reid, S. S. Huested, and J. Hering. 1984. Trace metals and radium in the Gulf of Mexico: An evaluation of river and continental shelf sources. Earth Planet. Sci. Lett. **69:** 69–87, doi:10.1016/0012-821X(84)90075-X

Brooks, G. R., L. J. Doyle, R. A. Davis, N. T. Dewitt, and B. C. Suthard. 2003. Patterns and controls of surface sediment distribution: West-central Florida inner shelf. Mar. Geol. **200:** 307–324, doi:10.1016/S0025-3227(03)00189-0

Burnett, W. C. 1998. Release of radium and other decay-series isotopes from Florida phosphate rock. Ph.D. thesis. Florida State Univ.

———, H. Bokuniewicz, M. Huettel, W. S. Moore, and M. Taniguchi. 2003. Groundwater and pore water inputs to the coastal zone. Biogeochemistry **66:** 3–33, doi:10.1023/B:BIOG.0000006066.21240.53

Cable, J. E., W. C. Burnett, J. P. Chanton, and G. L. Weatherly. 1996. Estimating groundwater discharge into the northeastern Gulf of Mexico using radon-222. Earth Planet. Sci. Lett. **144:** 591–604, doi:10.1016/S0012-821X(96)00173-2

Cai, W.-J. 2003. Riverine inorganic carbon flux and rate of biological uptake in the Mississippi River plume. Geophys. Res. Lett. **30:** 1032, doi:10.1029/2002GL016312

———. 2011. Estuarine and coastal ocean carbon paradox: CO_2 sinks or sites of terrestrial carbon incineration? Annu. Rev. Mar. Sci. **3:** 123–145, doi:10.1146/annurev-marine-120709-142723

———, Y.-C. Wang, J. Krest, and W. S. Moore. 2003. The geochemistry of dissolved inorganic carbon in a surficial groundwater aquifer in North Inlet, South Carolina, and the carbon fluxes to the coastal ocean. Geochim. Cosmochim. Acta **67:** 631–639, doi:10.1016/S0016-7037(02)01167-5

Charette, M. A., K. O. Buesseler, and J. E. Andrews. 2001. Utility of radium isotopes for evaluating the input and transport of groundwater-derived nitrogen to a Cape Cod estuary. Limnol. Oceanogr. **46:** 465–470, doi:10.4319/lo.2001.46.2.0465

———, P. B. Henderson, C. F. Breier, and Q. Liu. 2013. Submarine groundwater discharge in a river-dominated Florida estuary. Mar. Chem. **156:** 3–17, doi:10.1016/j.marchem.2013.04.001

Chipman, L. E. 2011. Oxygen and dissolved organic carbon dynamics in permeable coastal sediments. Ph.D. thesis. Florida State Univ.

Clark, C. D., and others. 2004. CDOM distribution and CO_2 production on the Southwest Florida Shelf. Mar. Chem. **89:** 145–167, doi:10.1016/j.marchem.2004.02.011

Coble, P. G., L. L. Robbins, K. L. Daly, W.-J. Cai, K. Fennel, and S. E. Lohrenz. 2010. A preliminary carbon budget for the Gulf of Mexico [Internet]. Fall 2010 issue of the Ocean Carbon and Biogeochemistry News. Woods Hole (MA): OCB Project Office [accessed August 2012]. Available from http://www.us-ocb.org/publications/OCB_NEWS_FALL10.pdf

Cyronak, T., I. R. Santos, D. V. Erler, and B. D. Eyre. 2013. Groundwater and porewater as major sources of alkalinity to a fringing coral reef lagoon (Muri Lagoon, Cook Islands). Biogeosciences **10:** 2467–2480, doi:10.5194/bg-10-2467-2013

Dickson, A. G. 1990. Standard potential of the reaction $AgCl(S)+1/2H_2(G)=Ag(S)+HCl(Aq)$, and the standard acidity constant of the ion HSO_4^- in synthetic sea water from 273.15K to 318.15K. J. Chem. Thermodyn. **22:** 113–127, doi:10.1016/0021-9614(90)90074-Z

Fanning, K. A., R. H. Byrne, J. A. Breland, II, P. R. Betzer, W. S. Moore, R. J. Elsinger, and T. E. Pyle. 1981. Geothermal springs of the West Florida continental shelf: Evidence for dolomitization and radionuclide enrichment. Earth Planet. Sci. Lett. **52:** 345–354, doi:10.1016/0012-821X(81)90188-6

Fleury, P., M. Bakalowicz, and G. De Marsily. 2007. Submarine springs and coastal karst aquifers: A review. J. Hydrol. **339:** 79–92, doi:10.1016/j.jhydrol.2007.03.009

Gagan, M. K., L. K. Ayliffe, B. N. Opdyke, D. Hopley, H. Scott-Gagan, and J. Cowley. 2002. Coral oxygen isotope evidence for recent groundwater fluxes to the Australian Great Barrier Reef. Geophys. Res. Lett. **29:** 1982, doi:10.1029/2002GL015336

Guo, X., and others. 2012. Carbon dynamics and community production in the Mississippi River plume. Limnol. Oceanogr. **57:** 1–17, doi:10.4319/lo.2012.57.1.0001

Hammerstrom, K. K., W. J. Kenworthy, M. S. Fonseca, and P. E. Whitfield. 2006. Seed bank, biomass, and productivity of *Halophila decipiens*, a deep water seagrass on the west Florida continental shelf. Aquat. Bot. **84:** 110–120, doi:10.1016/j.aquabot.2005.08.002

Hine, A. C., and others. 2008. Coral reefs, present and past, on the West Florida shelf and platform margin coral reefs of the USA, p. 127–173. *In* B. M. Riegl and R. E. Dodge [eds.], Coral reefs of the world. Springer.

Hitchcock, G. L., G. A. Vargo, and M.-L. Dickson. 2000. Plankton community composition, production, and respiration in relation to dissolved inorganic carbon on the West Florida Shelf, April 1996. J. Geophys. Res. **105:** 6579–6589, doi:10.1029/1998JC000293

Hsieh, Y.-T., W. Geibert, P. Van-Beek, H. Stahl, D. Aleynik, and G. M. Henderson. 2013. Using the radium quartet (^{228}Ra, ^{226}Ra, ^{224}Ra, and ^{223}Ra) to estimate water mixing and radium inputs in Loch Etive, Scotland. Limnol. Oceanogr. **58:** 1089–1102, doi:10.4319/lo.2013.58.3.1089

Jahnke, R. A., J. R. Nelson, R. L. Marinelli, and J. E. Eckman. 2000. Benthic flux of biogenic elements on the Southeastern US continental shelf: Influence of pore water advective transport and benthic microalgae. Cont. Shelf Res. **20:** 109–127, doi:10.1016/S0278-4343(99)00063-1

Jiang, L., S. Islam, W. Guo, A. S. Jutla, S. U. S. Senarath, B. H. Ramsay, and E. A. B. Eltahir. 2009. A satellite-based daily actual evapotranspiration estimation algorithm over South Florida. Global Planet. Change **67:** 62–67.

Johannes, R. E. 1980. The ecological significance of the submarine discharge of ground water. Mar. Ecol. Prog. Ser. **3:** 365–373, doi:10.3354/meps003365

Kelly, R. P., and S. B. Moran. 2002. Seasonal changes in groundwater input to a well-mixed estuary estimated using radium isotopes and implications for coastal nutrient budgets. Limnol. Oceanogr. **47:** 1796–1807, doi:10.4319/lo.2002.47.6.1796

Krumins, V., M. Gehlen, S. Arndt, P. Van Cappellen, and P. Regnier. 2013. Dissolved inorganic carbon and alkalinity fluxes from coastal marine sediments: Model estimates for different shelf environments and sensitivity to global change. Biogeosciences **10:** 371–398, doi:10.5194/bg-10-371-2013

Lee, Y. W., G. Kim, W. A. Lim, and D. W. Hwang. 2010. A relationship between submarine groundwater-borne nutrients traced by Ra isotopes and the intensity of dinoflagellate red-tides occurring in the southern sea of Korea. Limnol. Oceanogr. **55:** 1–10, doi:10.4319/lo.2010.55.1.0001

Lewis, E., and D. W. R. Wallace. 1998. Program developed for CO_2 system calculations. ORNL/CDLAC-105. Carbon Dioxide Information Analysis Center, Oak Ridge National Laboratory, U.S. Department of Energy.

Liu, Q., M. Dai, W. Chen, C. A. Huh, G. Wang, Q. Li, and M. A. Charette. 2012. How significant is submarine groundwater discharge and its associated dissolved inorganic carbon in a river-dominated shelf system? Biogeosciences **9:** 1777–1795, doi:10.5194/bg-9-1777-2012

Maher, D. T., I. R. Santos, L. Golsby-Smith, J. Gleeson, and B. D. Eyre. 2013. Groundwater-derived dissolved inorganic and organic carbon exports from a mangrove tidal creek: The missing mangrove carbon sink? Limnol. Oceanogr. **58:** 475–488, doi:10.4319/lo.2013.58.2.0475

Miller, R. L., T. F. Kraemer, and B. F. Mcpherson. 1990. Radium and radon in Charlotte Harbor Estuary, Florida. Estuar. Coast. Shelf Sci. **31:** 439–457, doi:10.1016/0272-7714(90)90037-R

Millero, F. J. 2005. Chemical oceanography. CRC Press.

———, T. B. Graham, F. Huang, H. Bustos-Serrano, and D. Pierrot. 2006. Dissociation constants of carbonic acid in seawater as a function of salinity and temperature. Mar. Chem. **100:** 80–94, doi:10.1016/j.marchem.2005.12.001

Moore, W. S. 1996. Large groundwater inputs to coastal waters revealed by ^{226}Ra enrichments. Nature **380:** 612–614, doi:10.1038/380612a0

———. 2000. Ages of continental shelf waters determined from ^{223}Ra and ^{224}Ra. J. Geophys. Res. **105:** 22117–22122, doi:10.1029/1999JC000289

———. 2007. Seasonal distribution and flux of radium isotopes on the southeastern U.S. continental shelf. J. Geophys. Res. **112:** C10013, doi:10.1029/2007JC004199

———. 2010. A reevaluation of submarine groundwater discharge along the southeastern coast of North America. Global Biogeochem. Cycles **24:** GB4005, doi:10.1029/2009GB003747

———, and R. Arnold. 1996. Measurement of ^{223}Ra and ^{224}Ra in coastal waters using a delayed coincidence counter. J. Geophys. Res. **101:** 1321–1329, doi:10.1029/95JC03139

———, J. O. Blanton, and S. B. Joye. 2006. Estimates of flushing times, submarine groundwater discharge, and nutrient fluxes to Okatee Estuary, South Carolina. J. Geophys. Res. **111:** C09006, doi:10.1029/2005JC003041

———, J. L. Sarmiento, and R. M. Key. 2008. Submarine groundwater discharge revealed by Ra-228 distribution in the upper Atlantic Ocean. Nat. Geosci. **1:** 309–311, doi:10.1038/ngeo183

Morey, S. L., P. J. Martin, J. J. O'Brien, A. A. Wallcraft, and J. Zavala-Hidalgo. 2003. Export pathways for river discharged fresh water in the northern Gulf of Mexico. J. Geophys. Res. **108:** C10, 3303, doi:10.1029/2002JC001674

Mucci, A. 1983. The solubility of calcite and aragonite in seawater at various salinities, temperatures, and one atmosphere total pressure. Am. J. Sci. **283:** 780–799, doi:10.2475/ajs.283.7.780

Najjar, R., and others. 2010. Carbon budget for the continental shelf of the eastern United States: A preliminary synthesis [Internet]. Winter 2010 issue of the Ocean Carbon and Biogeochemistry News. Woods Hole (MA): OCB Project Office [accessed May 2012]. Available from http://www.us-ocb.org/publications/OCB_NEWS_WINTER10.pdf

Officer, C. B. 1979. Discussion of the behaviour of nonconservative dissolved constituents in estuaries. Estuar. Coast. Mar. Sci. **9:** 91–94, doi:10.1016/0302-3524(79)90009-4

Phillips, N. E., D. A. Gettleson, and K. D. Spring. 1990. Benthic biological studies of the southwest Florida shelf. Am. Zool. **30:** 65–75.

Robbins, L. L., P. O. Knorr, X. Liu, R. Byrne, and E. A. Raabe. 2010*a*. USGS field activity 09FSH02 on the West Florida shelf, Gulf of Mexico, August 2009 [Internet]. U.S. Geological Survey Data Series 535, Part C. Reston (VA): U.S. Geological Survey [accessed September 2012]. Available from http://pubs.usgs.gov/ds/535/c/

———, ———, ———, ———, and ———. 2010*b*. USGS field activity 09FSH01 on the West Florida shelf, Gulf of Mexico, February 2009 [Internet]. U.S. Geological Survey Data Series 535, Part B. Reston (VA): U.S. Geological Survey [accessed September 2012]. Available from http://pubs.usgs.gov/ds/535/b/

Santos, I. R., D. T. Maher, and B. D. Eyre. 2012. Coupling automated radon and carbon dioxide measurements in coastal waters. Environ. Sci. Technol. **46:** 7685–7691, doi:10.1021/es301961b

Smith, C. G., and P. W. Swarzenski. 2012. An investigation of submarine groundwater-borne nutrient fluxes to the west Florida shelf and recurrent harmful algal blooms. Limnol. Oceanogr. **57:** 471–485, doi:10.4319/lo.2012.57.2.0471

Swarzenski, P. W., W. H. Orem, B. F. Mcpherson, M. Baskaran, and Y. Wan. 2006. Biogeochemical transport in the Loxahatchee River estuary, Florida: The role of submarine groundwater discharge. Mar. Chem. **101:** 248–265, doi:10.1016/j.marchem.2006.03.007

———, C. Reich, K. D. Kroeger, and M. Baskaran. 2007. Ra and Rn isotopes as natural tracers of submarine groundwater discharge. Mar. Chem. **104:** 69–84, doi:10.1016/j.marchem.2006.08.001

Vargo, G. A., K. L. Carder, W. Gregg, E. Shanley, C. Heil, K. A. Steidinger, and K. D. Haddad. 1987. The potential contribution of primary production by red tides to the West Florida Shelf ecosystem. Limnol. Oceanogr. **32:** 762–767, doi:10.4319/lo.1987.32.3.0762

Walsh, J. J., and others. 2003. Phytoplankton response to intrusions of slope water on the West Florida shelf: Models and observations. J. Geophys. Res. **108:** 3190, doi:10.1029/2002JC001406

Wanninkhof, R. 1992. Relationship between wind speed and gas exchange over the ocean. J. Geophys. Res. **97:** 7373–7382, doi:10.1029/92JC00188

Weisberg, R. H., Y. Liu, and D. A. Mayer. 2009. West Florida Shelf mean circulation observed with long-term moorings. Geophys. Res. Lett. **36:** L19610, doi:10.1029/2009GL040028

Weiss, R. F. 1974. Carbon dioxide in water and seawater: The solubility of a non-ideal gas. Mar. Chem. **2:** 203–215, doi:10.1016/0304-4203(74)90015-2

Windom, H. L., W. S. Moore, L. F. H. Niencheski, and R. A. Jahnke. 2006. Submarine groundwater discharge: A large, previously unrecognized source of dissolved iron to the South Atlantic Ocean. Mar. Chem. **102:** 252–266, doi:10.1016/j.marchem.2006.06.016

Yang, H., R. H. Weisberg, P. P. Niiler, W. Sturges, and W. Johnson. 1999. Lagrangian circulation and forbidden zone on the West Florida Shelf. Cont. Shelf Res. **19:** 1221–1245, doi:10.1016/S0278-4343(99)00021-7

Associate editor: H. Maurice Valett

Received: 04 October 2013
Accepted: 19 March 2014
Amended: 13 May 2014